National Technical University of Athens
School of Mechanical Engineering
Fluids Department
Parallel CFD & Optimization Unit

Preliminary Design of New Lubricants Featuring Inhomogeneous or Anisotropic Viscosity

Diploma Thesis

Georgios Bletsos

Academic Advisor:
Kyriakos C. Giannakoglou, Professor NTUA

Industrial Advisor:
Dr. Konstantinos Gkagkas, Expert Toyota Motor Europe

Athens, June 2019

Acknowledgements

First of all, I would like to express my deepest gratitude to my professor, K. Giannakoglou. Throughout my studies, he has been an inspiring figure not only for his immense knowledge but also for his dedication to teaching. I consider myself extremely fortunate to have been working under his academic supervision on this interesting topic.

Secondly, I would like to wholeheartedly thank my industrial supervisor Dr. K. Gkagkas. During my internship at Toyota Motor Europe, but also after, his guidance and advice have been indisputably of great importance. His enthusiasm towards science and engineering as well as his constant eagerness to discuss new and exciting ideas have been most inspiring for me. I would also like to thank the rest of the Advanced Technology Division for all the fruitful discussions they provided during my stay at Belgium.

I would also like to thank all the members of the research team of PCOpt/NTUA for always being eager to help when needed. In particular, I would like to express my most sincere gratitude to Dr. V. Asouti and Dr. E.M. Papoutsis-Kiachagias for always being available and happy to share some of their knowledge.

Last but not least, I would like to thank my family, for always being there for me with their love and support and my friends for being individually unique and authentic. I would also like to thank M.

Εθνικό Μετσόβιο Πολυτεχνείο
Σχολή Μηχανολόγων Μηχανικών
Τομέας Ρευστών
Μονάδα Παράλληλης Υπολογιστικής Ρευστοδυναμικής & Βελτιστοποίησης

Προκαταρτικός Σχεδιασμός Νέων Λιπαντικών με Ανομοιογενή ή Ανισότροπη Συνεκτικότητα

Διπλωματική Εργασία

Γεώργιος Μπλέτσος

Ακαδημαϊκός Επιβλέπων:
Κυριάκος Χ. Γιαννάκογλου, Καθηγητής ΕΜΠ

Βιομηχανικός Επιβλέπων:
Δρ. Κωνσταντίνος Γκαγκάς, Ειδικός Toyota Motor Europe

Αθήνα, Ιούνιος 2019

Περίληψη

Οι δυνάμεις τριβής αντιστοιχούν σε περίπου 15% της ενέργειας του καυσίμου που χάνεται στα οχήματα με μηχανές εσωτερικής καύσης. Για να μειωθεί το ποσοστό αυτό, πρέπει να σχεδιαστούν νέα λιπαντικά. Προηγούμενες μελέτες στα ιονικά υγρά και στους υγρούς κρυστάλλους αναδεικνύουν ανομοιογενείς ή ανισότροπες συμπεριφορές, αντίστοιχα. Με βάση τις μελέτες αυτές, η διπλωματική εργασία στοχεύει να μελετήσει τέτοιες συμπεριφορές με σκοπό την πιθανή βελτίωση των χαρακτηριστικών της λίπανσης.

Στη διπλωματική αυτή εργασία, η ανομοιογένεια προσομοιώνεται στον συνεχή χώρο με την εισαγωγή ενός εγγενούς ανομοιογενούς πεδίου συνεκτικότητας στις εξισώσεις Navier-Stokes. Προγραμματίζονται σχήματα παραμετροποίησης της συνεκτικότητας και εισάγονται στο περιβάλλον OpenFOAM. Με τη χρήση εξελικτικών αλγορίθμων μέσω του λογισμικού EASY, βελτιστοποιούνται τα πεδία συνεκτικότητας, με σκοπό τη μείωση των χαρακτηριστικών τριβής του λιπαντικού σε συνήθεις γεωμετρίες λίπανσης. Πραγματοποιούνται, επίσης, παραμετρικές μελέτες με σκοπό την καλύτερη κατανόηση

των φαινομένων που παρατηρούνται στις περιπτώσεις αυτές.

Η ανισότροπη συμπεριφορά προσεγγίζεται με τη χρήση τανυστικής συνεκτικότητας. Οι εξισώσεις Navier-Stokes τροποποιούνται για να συμπεριλάβουν τη νέα διατύπωση της συνεκτικότητας και δημιουργείται ένα αντίστοιχο μοντέλο το οποίο εισάγεται στο περιβάλλον OpenFOAM. Με τη χρήση του μοντέλου και εξελικτικών αλγορίθμων διερευνάται η επιρροή των όρων του τανυστή της συνεκτικότητας σε σχέση με την απόδοση του λιπαντικού.

Η μελέτη επεκτείνεται στην κλίμακα των νανομέτρων. Με τη χρήση προσομοιώσεων μοριακής δυναμικής, διαλέγονται τύποι σωματιδίων που παρουσιάζουν όμοιες ανομοιογένειες με αυτές που βρέθηκαν στον συνεχή χώρο. Με την κατάλληλη ρύθμιση των παραμέτρων που περιγράφουν τα σωματίδια, προσομοιώνονται ροές που παρουσιάζουν ανομοιογενή συνεκτικότητα. Παρατηρείται μείωση των δυνάμεων τριβής σε σχέση με ένα ομοιογενές ρευστό.

Το μεγαλύτερο μέρος αυτής της εργασίας πραγματοποιήθηκε στις εγκαταστάσεις της Toyota Motor Europe στις Βρυξέλλες, κατά τη διάρκεια ενιάμηνης πρακτικής άσκησης.

National Technical University of Athens
School of Mechanical Engineering
Fluids Department
Parallel CFD & Optimization Unit

Preliminary Design of New Lubricants Featuring Inhomogeneous or Anisotropic Viscosity

Diploma Thesis

Georgios Bletsos

Academic Advisor:
Kyriakos C. Giannakoglou, Professor NTUA

Industrial Advisor:
Dr. Konstantinos Gkagkas, Expert Toyota Motor Europe

Athens, June 2019

Abstract

Friction accounts for approximately 15% of fuel energy losses in internal combustion engine vehicles. To reduce it, new lubricants should be designed. Inspired by studies and observations on ionic liquids and liquid crystals, their inhomogeneous and anisotropic characteristics are studied as potential beneficial attributes to lubrication.

In this diploma thesis, inhomogeneity is emulated in the continuum domain by introducing an inherently inhomogeneous viscosity in the Navier-Stokes equations. Viscosity parameterization schemes are programmed and implemented in the OpenFOAM environment. Using an evolutionary algorithm, implemented within the generic optimization platform EASY, optimal viscosity profiles leading to a potential improvement in friction performance are identified for a converging hydrodynamic slider. Parametric studies are carried out to further understand the complexities involved in such lubricating methods.

In the anisotropic approach, a tensorial viscosity description is adopted. The Navier-Stokes equations are adapted accordingly and a model is programmed and included

in the OpenFOAM environment. The model is then coupled with an evolutionary algorithm targeting to identify the impact of the tensor's terms on lubrication performance.

The study is then extended to the nano-scale. Specific particle typologies, featuring optimized viscosity variations, as identified in the continuum domain, are selected using coarse grain molecular dynamics simulations. Through the appropriate tuning of the particles' properties, viscosity inhomogeneity is achieved and friction is reduced compared to a homogeneous case.

Major part in this diploma thesis was carried out in the premises of Toyota Motor Europe in Brussels, Belgium, during a 9 month long internship.

Acronyms

NTUA	National Technical University of Athens
PCopt	Parallel CFD& Optimization Unit
TME	Toyota Motor Europe
OpenFOAM	Open Field Operation and Manapulation
LAMMPS	Large-scale Atomic/Molecular Massively Parallel Simulator
FVM	Finite Volume Method
PDE	Partial Differential Equation
CFD	Computational Fluid Dynamics
MD	Molecular Dynamics
EA	Evolutionary Algorithms
EASY	Evolutionary Algorithms System
w.r.t.	with respect to
N-S	Navier-Stokes equations

Contents

Chapter 1

Introduction

Tribology [1] is the science of interacting surfaces in relative motion. It includes the study and application of the principles of friction, *lubrication* and wear. Tribology is highly interdisciplinary in nature and draws upon several academic areas including: physics, chemistry, materials science and engineering.

While tribology can be considered a rather new field of study, its worldwide importance is considerable. In 2017, K. Holmberg and A. Erdemir [2] attempted to quantify the impact of friction, wear and energy consumption worldwide. Some of their conclusions are the following:

- In total, 23% of the world's total energy consumption originates from tribological contacts. Of that, 20% is used to overcome friction and 3% is used to remanufacture worn parts.

- By taking advantage of the new surface, materials, and lubrication technologies for friction reduction and wear protection in vehicles, machinery and other equipment worldwide, energy losses due to friction and wear could potentially be reduced by 40% in the long term (15 years).

Taking the above into consideration, research on the field of tribology and optimization of the lubrication materials is a matter of interest for the automotive industry but also for the worldwide community aiming to reduce the total energy consumption.

1.1 Lubrication

Lubrication is one of the key areas involved in the science of tribology. It is the process or technique employed to reduce friction between, and wear of one or both, surfaces in proximity and moving relative to each other, by interposing a substance called lubricant in between them. It can be divided in three general categories:

1. **Boundary lubrication**, where the solid surfaces come into direct contact and the load is supported mainly by surface asperities. It is characterized by high friction.
2. **Mixed lubrication**, where partial asperity contact exists and the load is supported by both the lubricant and asperities.
3. **Hydrodynamic lubrication**, where the asperity contact is negligible and the load is supported by mainly the lubricant.

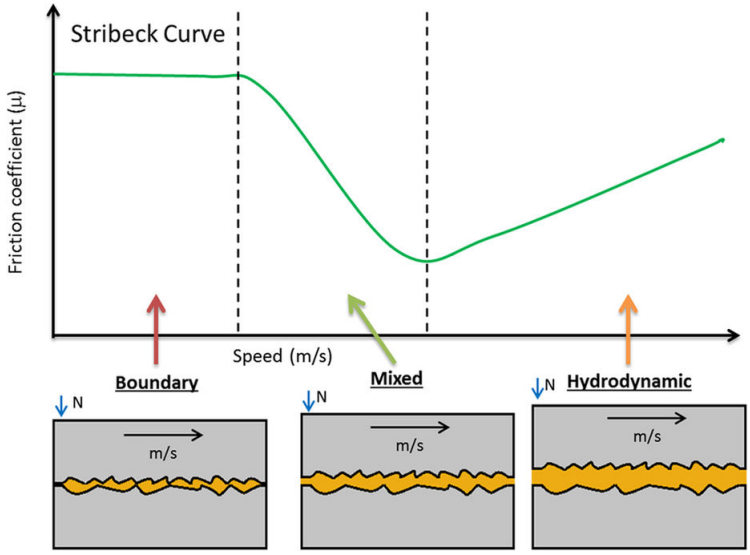

Figure 1.1: *Stribeck curve. It is used to determine in which regime of lubrication the component is functioning depending on the relative speed of its surfaces [3].*

This diploma thesis is exclusively dealing with **hydrodynamic lubrication**.

1.1.1 Hydrodynamic Lubrication

Hydrodynamic lubrication or fluid film lubrication occurs when a viscous fluid has the ability to separate two inclined surfaces in relative motion, by developing hydrodynamic pressure in a thin lubricating film. In order for the fluid film to sustain

the ability of separating the two surfaces, it is of utmost importance that one of the two surfaces be inclined as seen in fig. 1.2.

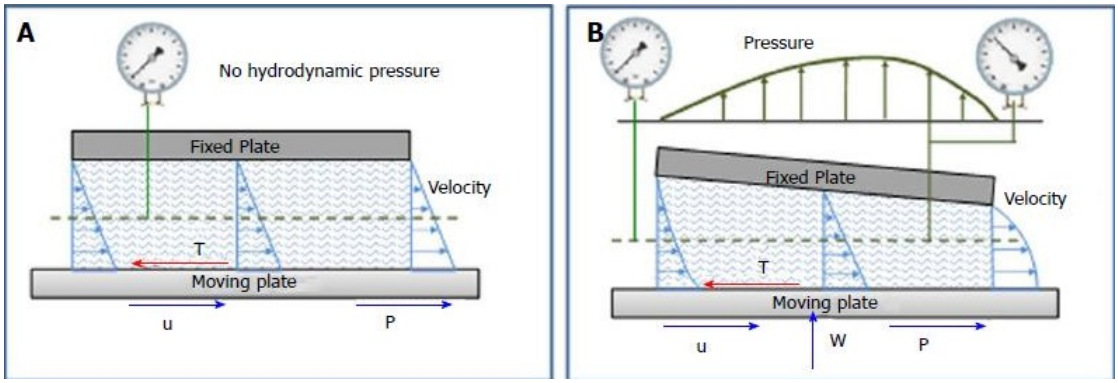

Figure 1.2: *Couette flow in A, where hydrodynamic pressure isn't developed. Hydrodynamic lubrication slider in B [4].*

The most used mathematical equation describing this phenomenon is the Reynolds equation [5], which is an integrated version of the N-S across the film thickness. However, there are some inherent limitations in the Reynolds approach. Gradients of fluid properties and velocity across the film thickness are either assumed to be zero or greatly simplified. On the other hand, with a CFD approach to hydrodynamic lubrication, it is possible to resolve all gradients across the film which is necessary on a non-homogeneous or anisotropic approach of the fluid properties. One of the necessary assumptions for the Reynolds equation involve constant viscosity of the lubricant throughout the fluid domain. This assumption is contrasted with the scope of the work set for this diploma thesis and, thus, the governing equations of the steady, laminar flow are the N-S for an incompressible fluid.

1.2 Lubrication in Internal Combustion Engines

A conventional internal combustion engine is comprised of dozens of moving parts. Without proper oiling, these parts may run against each other with tremendous speed, creating friction which then leads to heat. This heat can wear the mechanical parts of an engine. Worn parts due to friction lead to increased emissions since the engine is pushed to work harder. Improvement of the tribology systems found in an internal combustion engine, through novel lubrication techniques, is, therefore, necessary for an automotive company. In this section, several mechanical components where friction is present are briefly discussed.

1.2.1 Piston Rings

Piston rings are circular metallic rings placed around the piston with a certain pretension, and their main purpose is to isolate the combustion chamber volume with minimum friction. A typical sketch of a piston with its piston rings can be seen in 1.3.

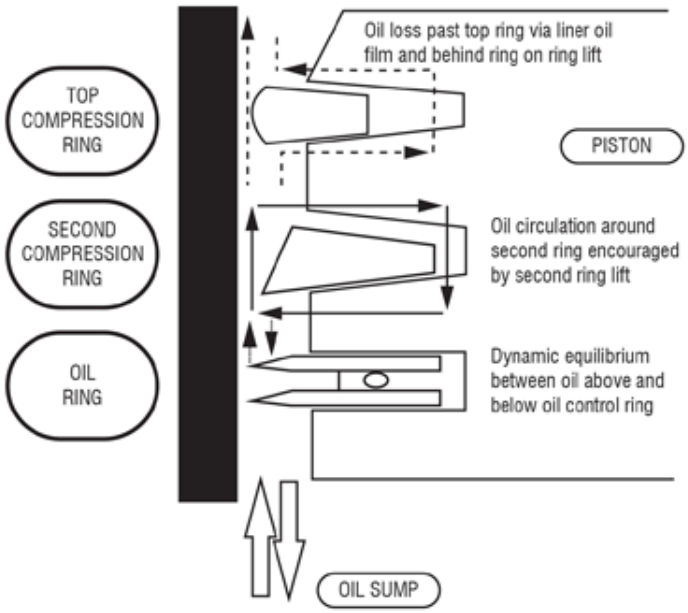

Figure 1.3: *Sketch of a piston ring-pack operation. Engine oil is designed to produce an oil film on the cylinder wall. A thin film should remain throughout the operation of the engine [6].*

The main purpose of piston rings is to keep gas blow-by from the combustion chamber to the crankcase to a minimum. The combustion gases can flow past the piston ring from three locations, the piston ring gap, the front face of the ring and its backside. Piston rings seal the gas by expanding outwards towards the liner due to the gas pressure acting on their back and the pretension force.

Piston rings also spread the lubricating oil up and down the liner uniformly and at the same time scrape off the excessive oil and return it to the crankcase during the downstroke.

Piston rings also stabilize the piston, preventing it from coming into contact with the liner, especially during cold starts. While the piston moves along the liner, the piston ring creates a thin lubricating film between it and the liner, preventing metal to metal contact [7].

1.2.2 Journal Bearings

Journal bearings [1] are mechanical components appearing in the majority of engineering applications. They are used either to support the radial load of a rotating shaft or simply as a guide for the smooth transmission of torque with minimum both power loss and wear. The geometry of a journal bearing consists of a hollow cylinder, enclosing a solid shaft that rotates about its axis. The bearing cylinder is usually held stationary. The hydrodynamic film which supports the radial load is generated between the surfaces of the rotating shaft and the stationary bearing. A typical sketch of a journal bearing during operation, including the developed hydrodynamic film is shown in 1.4.

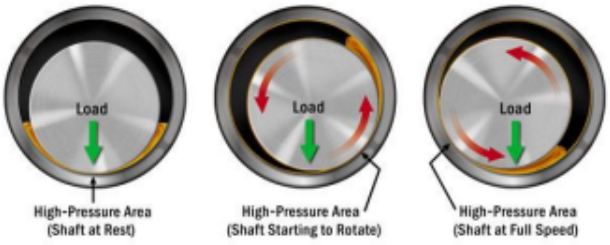

Figure 1.4: *Journal bearing sketch with the developed oil film [8].*

1.3 Literature Review and Outline of the Thesis

In engineering applications, there is always a drive for reduced emissions, reduced wear, increased service intervals and last but not least, reduced friction. A deeper understanding of lubrication mechanisms as well as how to accurately model them is, thus, necessary prior to proposing new lubricant design concepts.

A proposed solution is the use of ionic liquids (ILs) in the next generation of lubricants [9]. Over the last decades, the field of computational lubricated nanotribology has been well established [10, 11] allowing the application of such methods in studies of ILs [12, 13]. At the same time, a large number of experimental studies of ILs as base lubricants [14, 15] or lubricant additives [16, 17] has shown good potential, with friction reduction up to 55% [18] compared to conventional hydrocarbon oils. One of the observations made from both computational and experimental studies is that, under confinement, the liquid exhibits a layering behaviour as well as near-wall solidification. It is assumed that significant friction reduction is due to the inherent ability of the molecules to react with the metallic surfaces and form a lubricative boundary tribo-film [18].

In previous studies, inhomogeneities have been studied using molecular dynamics (MD) simulations, in sheared ultrathin lubricating films, reporting a highly viscous, adsorbed layer in contact with a less viscous fluid layer, within the film [19]. The findings are in agreement with Surface Forces Apparatus experiments [20, 21] concluding that films with inhomogeneities, due to the existence of regions with dramatically different viscosities, exist.

Most of the studies target at resolving features and complexities on the nano-scale while macro-scale models fall short on studying the nuances of the phenomena involved. An apparent disparity between the fields of expertise relevant to the highly interdisciplinary topic of tribology is, thus, created [22]. Recent works address complex phenomena across the scales [23] while others present hybrid atomistic-continuum models capable of resolving nano-scale features of fluid flow [24]. Coherent analysis across the scales and disciplines is shown to be necessary for a deeper understanding of the lubrication complexities.

Driven by the observations made in studies on ILs, as well as other studies reporting coexistence of layers with different rheological behaviour within the same film, inhomogeneity and anisotropy is studied herein, targeting to identify through the use of CFD-based optimization optimal patterns beneficial to lubrication. The contents of this diploma thesis are outlined as follows:

- Chapter 2: The flow equations, the geometry under investigation as well as the optimization method are presented. A case of isotropic and homogeneous fluid properties is presented to validate the CFD results by comparing them with data from literature on similar problems.
- Chapter 3: Fluids with inhomogeneous viscosity in the geometry's longitudinal and transversal directions are studied, respectively. Results are presented and discussed.
- Chapter 4: Anisotropic fluids are modeled through the implementation of a tensorial viscosity in the flow equations. Results are presented and discussed.
- Chapter 5: Based on the optimal transversal viscosity distribution identified in the continuum domain, the study is extended towards the atomistic domain, where through the use of coarse grain molecular dynamics (MD) simulations, an identification of particle typologies that exhibit similar viscosity variations is sought.
- Chapter 6: This work is summarised and conclusions are drawn.

Chapter 2

Governing Equations & Optimization

2.1 Governing Equations

The problem under investigation is governed by the N-S equations for an incompressible fluid in a steady, laminar flow. The equations to be solved are the conservation of mass and momentum, namely the continuity (eq. 2.1) and momentum (eq. 2.2) equations, respectively.

$$R^p = \frac{\partial v_i}{\partial x_i} = 0 \tag{2.1}$$

$$R_i^u = v_j \frac{\partial v_i}{\partial x_j} - \frac{\partial}{\partial x_j}\Big[\nu\Big(\frac{\partial v_i}{\partial x_j} + \frac{\partial v_j}{\partial x_i}\Big)\Big] + \frac{\partial p}{\partial x_i} = 0 \tag{2.2}$$

where i,j=1,2 for a 2D analysis, ν is the kinematic viscosity, p is the pressure divided by the density and v_i the velocity components. In the cases of inherently, inhomogeneous viscosity media, kinematic viscosity is distributed throughout the flow domain and differentiated accordingly. In contrast, in an anisotropic fluid, kinematic viscosity is described by a, constant in space, tensor.

2.2 Geometry

The geometry under investigation is that of a converging hydrodynamic slider, fig. 2.1, unless stated otherwise. The computational domain is discretized using a structured grid with approximately 12000 computational cells.

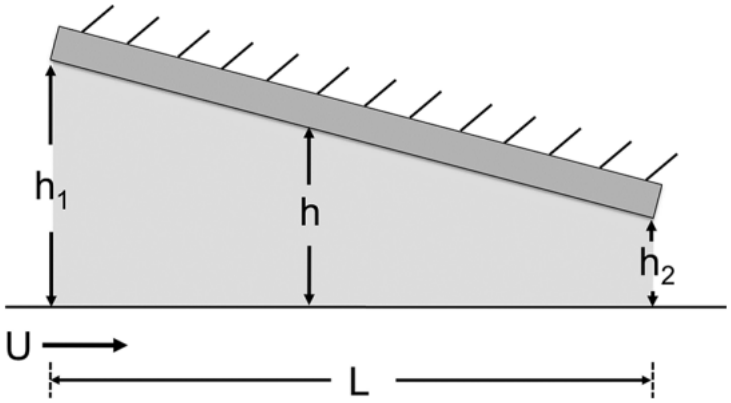

Figure 2.1: *Sketch of a typical converging hydrodynamic slider geometry [25].*

Parameters of fig. 2.1 correspond to $L = 1\ mm$, $h_1 = 2.2\ \mu m$, $h_2 = 1.0\ \mu m$ and $U = 1\ m/s$. The corresponding values are decided in order to match a common configuration for hydrodynamic lubrication applications. As this diploma thesis targets at the design of lubricants, the geometrical parameters are not investigated further.

2.3 Finite Volume Method

Equations 2.1 & 2.2 are discretized using the finite volume method (FVM). FVM [26] is a method for representing and evaluating partial differential equations in the form of algebraic equations. Similar to the finite difference method or finite element method, values are calculated at discrete places on a meshed geometry. The FVM subdivides the flow domain into a finite number of smaller non-overlapping control volumes. The transport equations are, then, integrated over each of these control volumes by approximating fluxes with appropriate differencing schemes.

The geometry is discritized into a number of cells, or control volumes, through the use of a structured grid. These are contiguous, meaning that they do not overlap one another and fill the domain completely. Generally, variables are stored at the cell centres. After the computational grid is generated, the system of the partial

differential equations (PDEs) is transformed into algebraic expressions which can be expressed as

$$\mathbf{M}\ \lambda = \mathbf{b} \tag{2.3}$$

where λ is the vector of the dependent variable and $\mathbf{b}$ the source vector. Finite volume discretization of each term is formulated by integrating the term over a cell volume V. Since the flow PDEs are non-linear, matrix M depends on λ and a first step for its numerical solution is to linearise it. This gives rise to a solution scheme based on an iteratively used linear solver (either explicit or implicit). The above methodology is carried out through the use of a pressure-based algorithm, namely the SIMPLE algorithm, within OpenFOAM [27].

2.3.1 Boundary Conditions

In order to solve the problem, boundary conditions for each independent variable at each boundary patch of the grid should be defined. The two main boundary condition types are:

1. **Dirichlet**, prescribes the value of the variable on the boundary.
2. **Neumann**, prescribes the gradient of the variable normal to the boundary.

In specific, a zero Neumann condition for the pressure is imposed along the top and bottom walls, while inlet and outlet are held at constant pressure (zero Dirichlet). While zero pressure is unphysical, from an engineering point of view, it is used herein considering that the fluid is incompressible and therefore computation of only the derivatives of pressure is required. Therefore, a zero pressure, in terms of boundary conditions, could theoretically correspond to any given value. For the velocity, no-slip conditions (equivalent to Dirichlet condition) are imposed along the walls, with the bottom one moving while the top one being stationary, and zero Neumann conditions at the inlet and outlet.

2.3.2 The SIMPLE algorithm

In what follows, the variant of the SIMPLE algorithm, for the solution of the primal equations is briefly presented [28].

The momentum equations, 2.2, can be written in a semi-discretized form as

$$a_P v_{P,i} = \sum_{N=1}^{NB(P)} a_N v_{N,i} - \frac{\partial p}{\partial x_i} \tag{2.4}$$

where P is used to denote both the cell index and its centroid in which the momentum equations are discretized and $NB(P)$ are its adjacent cells, fig. 2.2. The coefficients a_P and a_N result from the discretization of the convection and diffusion terms. It is assumed that the coefficient a_P is the same for all the components of the momentum equations. The iterative solution of eq. 2.4 using the pressure field p^*, obtained through the previous iteration results in a velocity field, v^*, which does not necessarily satisfy the continuity equation. However, no equation in which the pressure field is updated exists so far. For that reason, an equation, in which pressure is computed and velocity corrected, needs to be derived.

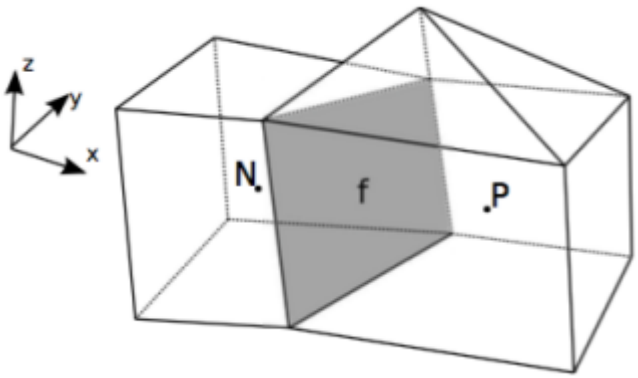

Figure 2.2: *Mesh cell, centered at P and one of its adjacent mesh cells centered at N. The two cells share a single face f [28].*

Let the velocity and pressure fields that satisfy the momentum and continuity equations be denoted as v_i and p, respectively. The semi-discretized eq. 2.4 can be written as

$$a_P v^*_{P,i} = \sum_{N=1}^{NB(P)} a_N v^*_{N,i} - \frac{\partial p^*}{\partial x_i} \tag{2.5}$$

Once the above equation is solved in the current iteration of the solution algorithm, a prediction of the velocity components is given by

$$v^*_{P,j} = \hat{v}_{P,j} - \frac{1}{a_P}\frac{\partial p^*}{\partial x_j} \tag{2.6}$$

where

$$\hat{v}_{P,j} = \frac{1}{a_P} H_{P,j}(\nu^*) \tag{2.7}$$

$$H_{P,j}(\nu^*) = \sum_{N=1}^{NB(P)} a_N v^*_{N,j} \tag{2.8}$$

Subtracting eq. 2.6 from 2.4 and assuming that coefficients (a_P, a_N) are approximately the same, the following equation holds

$$a_P v'_{P,i} = \sum_{N=1}^{NB(P)} a_N v'_{N,i} - \frac{\partial p'}{\partial x_i} \tag{2.9}$$

in which v' and p' correspond to the velocity and pressure corrections that need to be added to v^* and p^*, respectively, in order to also satisfy the continuity equation.

An assumption made by SIMPLE is that the first term on the right hand side of eq. 2.9 is negligible compared to the gradient of the pressure correction. Therefore, eq. 2.9 is simplified to

$$v'_{P,i} = -\frac{1}{a_P} \frac{\partial p'}{\partial x_i} \tag{2.10}$$

From the continuity equation one can also derive the following

$$\frac{\partial v_j}{\partial x_j} = 0 \Rightarrow \frac{\partial v'_j}{\partial x_j} = -\frac{\partial v^*_j}{\partial x_j} \tag{2.11}$$

and by substituting 2.10 into 2.11 yields

$$\frac{\partial}{\partial x_j}\Big(\frac{1}{a_P} \frac{\partial p'}{\partial x_j}\Big) = \frac{\partial v^*_j}{\partial x_j} \tag{2.12}$$

Equation 2.12 can be further processed after taking eq. 2.6 into account

$$\frac{\partial}{\partial x_j}\Big(\frac{1}{a_P}\frac{\partial p'}{\partial x_j}\Big) = \frac{\partial}{\partial x_j}\Big(\hat{v}_{P,j} - \frac{1}{a_P}\frac{\partial p^*}{\partial x_j}\Big) \Rightarrow \tag{2.13}$$

$$\frac{\partial}{\partial x_j}\Big(\frac{1}{a_P}\frac{\partial p}{\partial x_j}\Big) = \frac{\partial \hat{v}_{P,j}}{\partial x_j} \tag{2.14}$$

giving rise to the pressure equation. Further analysis related to the computation of the volume flux, m_f and skew correction can be found in [28].

The steps of the SIMPLE algorithm are as follows:

1. Solve eq. 2.5 to acquire the velocity field, v^*, based on the pressure and velocity fields of the previous iteration (or the boundary conditions).
2. Compute $\hat{v}_{P,i}$ through eq. 2.7 and interpolate its values to the cell faces.
3. Compute the pressure field through eq. 2.14.
4. Update the volume flux m_f.
5. Explicitly relax the pressure field.
6. Update the velocity field v_i at the cell centres using the relaxed pressure gradient.
7. Update the turbulence model equations, if turbulence is activated.
8. If the desired level of convergence is met for all equations, terminate the run. Otherwise, go to step 1.

2.4 Evolutionary Algorithms

Optimization methods [29] can be split into two main categories, gradient-based (deterministic) methods and stochastic methods. Deterministic optimization methods use the general definition of the derivative of the objective function, which is required to be computed. On the other hand, stochastic methods, as the name suggests, are using randomised search to find the optimal solution. It is clear, therefore, that in order to use a deterministic method the computation of the derivatives of the objective function is necessary w.r.t. the design variables.

Evolutionary algorithms are the main representatives of the stochastic methods. They are based on principles derived from natural evolution, such as reproduction, mutation, recombination and selection. Basic characteristic of this method, in contrast with other stochastic methods, is that it uses a population of candidate solu-

tions (population-based methods) instead of a single solution in every optimization iteration. The principles of natural evolution, mentioned above, can be translated into mathematical operators. The evolution of the population takes place after the repeated application of these operators with the goal of driving a population of candidate solutions towards better regions of the search space w.r.t. the selected objective function.
The main characteristics of an evolutionary algorithm can be summarized by the following

- They use populations of individuals (candidate solutions) which evolve simultaneously, instead of single individuals.
- The evolution of the population is determined by the objective function values of its individuals.
- Populations must change dynamically by creating new individuals and eliminating other depending on their objective function value.
- During the evolution of the population, hereditary operations are employed. Features of the parent population should be found in the offspring population but new features must also appear.

Like every optimization method, evolutionary algorithms have both advantages and disadvantages in comparison with other methods.

One great disadvantage of an evolutionary algorithm, in its standard form, is that it requires a, relatively, large number of evaluations to identify the optimal solution. Therefore, the evaluation software, which is the 'expensive' part of the optimization procedure, must be used a lot of times. Another disadvantage is that the more the design variables, the more the evaluations needed to actually find the optimal solution. Therefore, the computational cost greatly increases with the increase of the design variables. Nevertheless, there are methods that can reduce the total number of evaluations thus decreasing the total cost/time of an optimization procedure. Such a method is a metamodel assisted evolutionary algorithm. Metamodels replicate costly calls to the CFD evaluation software, by approximating the objective function at negligible cost, after training them on data collected from candidate solutions already evaluated, on the CFD tool, during the evolution.

On the other hand, evolutionary algorithms in contrast with deterministic methods will always find the global optimum of the problem, provided that an "infinite" number of evaluations can be performed. Another advantage is that, as already mentioned, an evolutionary algorithm can be used directly in a new problem without changing anything on the optimization software to fit the problem requirements. The only requirement for an evolutionary algorithm to function is an output from the evaluation software with the value/s of the objective function/s for the individual to be evaluated.

Weighting the advantages and disadvantages of each optimization method it is de-

cided that an EA better fits the requirements of the problem.

2.4.1 EA-Based Optimization

The EA-based optimization [29] can be summarized in the following steps

1. Basic parameters, such as the size of the parent and offspring population, are selected, depending on the problem. The symbols $S^{g,\mu}$ and $S^{g,\lambda}$ correspond to the parent and offspring population, respectively. Letter g refers to the generation count. The procedure begins with a random selection of the individuals of $S^{0,\lambda}$.

2. The λ individuals of $S^{g,\lambda}$ are evaluated through the use of an evaluation software. After the flow fields are computed, a post-processor is used to calculate the objective function of each individual.

3. The members of the elite population denoted by $S^{g,e}$ are renewed by the members of $S^{g,\lambda}$ that have a better objective function value. This step can be expressed as:

$$S^{g+1,e} = T_e(S^{g,\lambda} \cup S^{g,e}) \tag{2.15}$$

   where T_e is the operator identifying elite members.

   There is always a chance that, at this step, no individual of $S^{g,\lambda}$ is better than the ones of $S^{g,e}$ and, therefore, the population of the elites remain the same. This is an indication that the EA didn't manage to find a better solution in the last iteration.

4. The elitism operator, T_{e2}, is used to replace individuals of $S^{g,\lambda}$ by individuals of $S^{g,e}$. Usually the worst individuals of the offspring population are chosen. Depending on the value of this operator, the search engine can be more elitistic or less elitistic. Through this step, getting a new generation (iteration) with an optimal solution worse than the one of the previous one, is avoided. This step can be expressed as:

$$S^{g,\lambda} = T_{e2}(S^{g,\lambda} \cup S^{g+1,e}) \tag{2.16}$$

5. The new parent population $S^{g+1,\mu}$ is created through the use of the operator T_μ. Usually this is done through the use of the current offspring and parent population

$$S^{g+1,\mu} = T_\mu(S^{g,\mu} \cup S^{g,\lambda}) \tag{2.17}$$

6. The next step is the generation of a new offspring population, $S^{g+1,\lambda}$. To accomplish this, individuals of $S^{g+1,\mu}$ and $S^{g+1,e}$ are randomly selected. For each combination of parents selected some operators, such as the mutation operator (T_m) and crossover operator (T_r), are used to produce the final offspring population of the new generation.

$$S^{g+1,\lambda} = T_m(T_r(S^{g+1,\mu} \cup S^{g+1,e}) \tag{2.18}$$

7. Convergence criteria for a single objective optimization, such as the optimal value remaining the same for N generations, are checked and, if satisfied, the algorithm stops. If not, a new generation begins by repeating steps 2 to 6.

2.4.2 EASY

EASY [30] is a general purpose optimization platform developed by PCopt of NTUA. It can be used for single-(SOO) and multi-objective (MOO), constrained or unconstrained optimization problems.

EASY offers a variety of options, such as hybrid optimization (using both stochastic and gradient-based optimization techniques), metamodel assisted evolutionary algorithms and more. Most importantly, though, EASY is enabled for cluster and grid-computing.

In the cases to be presented, the evaluation cost is small due to the simplicity of both the geometry and the equations needed to be solved. Therefore, running the solver of the governing equations in parallel would make little to no sense. On the other hand the procedure sketched on 2.4.1 can be parallelized with great profit on the time needed for the procedure to finish. Each evaluation can be computed at one CPU independently of any other through the use of a cluster, provided by TME.

EASY is a synchronous EA, i.e. there is a sychronization barrier at the end of each generation. The software does not proceed to a new generation if all the evaluations of the previous one have not been completed.

Assuming that for a different set of design variables the evaluation time remains almost the same and if the number of CPUs occupied by EASY are equal to the offspring population, then one generation will be computed in clock time equal to that of a single evaluation.

2.5 Performance Parameters

The optimization procedure targets at either minimizing or maximizing an objective function. After the numerical solution of the N-S, the flow fields p and v_i become available and these should be post-processed to compute the parameters that characterize the efficiency of a lubricant. In hydrodynamic lubrication, two are the performance parameters of interest.

- **Friction** between the lubricant and the lubricated surface, that is the total force acting on the tangential direction of the surface. It is a quantity to be minimized.

- **Load capacity**, that is the total force acting on the normal direction of the surface. Load capacity is to be maximized.

A post-processor is developed within OpenFOAM to compute the aforementioned quantities.

Friction force is obtained by integrating τ_{xy} along the longitudinal direction of the slider. Although friction appears on both surfaces, the most affected surface is the moving one, namely the bottom horizontal wall as shown in fig. 2.1. Following the above, friction on the bottom horizontal wall is defined as :

$$F = \int_0^L \tau_{xy} dx = \int_0^L \nu(\frac{\partial u_x}{\partial y} + \frac{\partial u_y}{\partial x})dx \tag{2.19}$$

Since no-slip condition is imposed for the velocity components on the walls, $\frac{\partial u_y}{\partial x}$ can be neglected. This quantity is to be minimized since it is associated with wear of the lubricated components and energy losses.

Load capacity is the parameter that quantifies the force that can be implemented on the normal direction of the components without squeeze film phenomenon, where the two components start moving towards each other and the fluid moves outside of the lubricated area. This parameter can be obtained by integrating the pressure distribution along the longitudinal direction

$$W = \int_0^L p dx \tag{2.20}$$

This quantity is to be maximised in order to develop a lubricant that can sustain bigger forces without the squeeze film phenomenon.

In order to avoid a multi-objective optimization problem, a synthetic objective function is defined. The specific friction

$$SF = \frac{F}{W} \tag{2.21}$$

of the bottom wall is used as a single function to be minimized during the optimization.

2.6 Isotropic-Homogeneous Viscosity Case

The terms of isotropy and homogeneity in physics are defined as following:

- Isotropy is uniformity in all directions. In the study of mechanical properties of materials, *isotropic* means having identical values of a property in all directions. So, isotropic viscosity of a fluid means that the measurement of viscosity, in a specific point in space, is independent of the orientation of the measurement.
- An *homogeneous* material has the same properties at every point in space. Therefore, a fluid with homogeneous viscosity can be considered having the same value of viscosity irrespective of where the measurement takes place.

The definitions of *anisotropic* and *inhomogeneous* can be derived by considering the exact opposite of the above definitions.

In order to understand the value of implementing continuum models that consider the properties of the analysed medium to be either anisotropic or inhomogeneous, a comparison metric is due. Therefore, in this section, the parameters of interest are computed using CFD and validated using data from literature, for an isotropic and homogeneous fluid, thus validating the model accuracy and creating a comparison measure for what follows.

For the CFD simulations, a kinematic viscosity $\nu = 3{\cdot}10^{-6}\ \frac{m^2}{s}$ is used, corresponding to a common engine oil at 373 K. The convergence history of the simulation is shown in fig. 2.3 . As can be seen, the grid as well as the solution scheme used to simulate the homogeneous-isotropic viscosity case is able to converge in less than 5000 iterations.

Through the use of the developed post-processor, the performance parameters of the lubricant are computed and compared with equivalent results in the literature [1], as shown in table 2.1. A small difference of 4% is noted for the friction and load capacity results. In the literature, the equation used to describe the problem is the Reynolds equation which is expected to lead to a small error compared to the

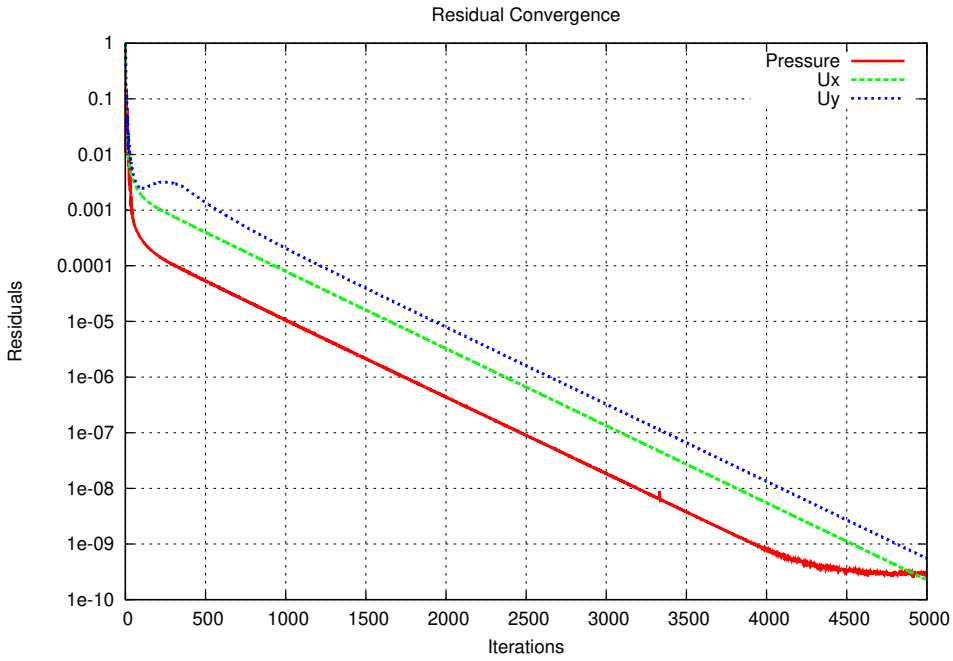

Figure 2.3: *Non-dimensional residuals of the discretized N-S reduced more than 9 orders of magnitude.*

results of the N-S analysis. However, the results are deemed satisfactory and the model validated. The CFD results are to be used as a comparison metric to what follows.

Table 2.1: *Performance parameters for lubricant with* $\nu = 3 \cdot 10^{-6}\ \frac{m^2}{s}$. *Comparison between CFD and literature [1]. Parameters* F_h, W_h, SF_h *correspond to the computed values from CFD.*

Performance Parameters	CFD	Literature
Friction	F_h	$0.96F_h$
Load Capacity	W_h	$0.96W_h$
Specific Friction	SF_h	SF_h

Chapter 3

Inhomogeneous Viscosity

While the properties of a material are usually assumed homogeneous, this is not always true. Nanoscale analysis of certain materials shows that the behaviour of the material can vary in space. In lubrication, inhomogeneities can be caused due to the inherent ability of the lubricant's molecules to interact differently with the lubricated walls or by external causes such as electric/magnetic fields. In this chapter, inhomogeneity is studied as a potential beneficial attribute to modern lubricants. This characteristic is emulated in a continuum approach by introducing an inhomogeneous viscosity field in the N-S equations. To exploit the aforementioned behaviour for the specific friction minimization, the viscosity field is optimized.
This chapter is split into the following sections :

- Viscosity is distributed along the longitudinal direction of the geometry with the use of a Bézier curve. The curve is optimized w.r.t. the values of the three control points. Results are presented and discussed.

- Viscosity is distributed along the transversal direction of the geometry with the use of a piecewise linear interpolation scheme. The optimal viscosity configuration is tested in different geometries to investigate the sensitivity of the result to different tribological configurations. Results are presented and discussed.

To perform the above, the OpenFOAM environment is enriched with appropriate viscosity parameterization pre-processors.

3.1 Viscosity Varying in the Longitudinal Direction

Prior to the solution of eqs. 2.1 & 2.2, the kinematic viscosity field needs to be parameterized. In this section, interest is given to the impact of a non-uniform viscosity distribution along the longitudinal direction. Thus, a parameterization scheme of the form $\nu = \nu(x)$ is required. This is realized through the use of a quadratic Bézier curve.

3.1.1 Bézier Curve

In contrast to already existent viscosity schemes of Non-Newtonian fluids, the viscosity parameterization scheme used herein is a pre-processor and does not renew the viscosity values of each computational cell throughout the solution of the flow equations.

A Bézier curve on the (x, ν) plane is used to parameterize viscosity along the longitudinal direction. It is a parametric curve that is defined by a set of control points $\mathbf{P}_0$ through $\mathbf{P}_n$, where n is called its order. The first and last control points are always the end points of the curve; however, the intermediate control points generally do not lie on the curve.

An explicit definition expresses the n^{th} degree Bézier curve as follows:

$$\mathbf{B}(t) = \sum_{i=0}^{n} \binom{n}{i} (1-t)^{n-i} t^i \mathbf{P}_i \tag{3.1}$$

where $\binom{n}{i}$ are the binomial coefficients and t is a non-dimensional parameter with values from 0 to 1. For a quadratic Bézier curve with $n = 2$, eq. 3.1 takes the following form:

$$\mathbf{B}(t) = (1-t)^2 \mathbf{P}_0 + 2(1-t)t\mathbf{P}_1 + t^2 \mathbf{P}_2 \tag{3.2}$$

Since interest is given on parameterizing ν, the problem is 1D and thus the control points of eq. 3.2 are scalar values and can be written as P_0, P_1 and P_2. An optimization could now start with the control points being the design variables and $t = \frac{x}{L}$, where L is the length of the hydrodynamic slider. However, an optimal distribution of t is also sought, thus providing extra control to the final viscosity curve. In order

to achieve this, the x coordinates of the grid are also described by a quadratic Bézier curve, as follows:

$$x = (1-t)^2 x_0 + 2(1-t)t x_1 + t^2 x_2 \tag{3.3}$$

By setting $x_0 = 0$ and $x_2 = L$, we end up with

$$\begin{aligned} t^2(L - 2x_1) + 2x_1 t - x &= 0 \\ t^2(1 - 2\frac{x_1}{L}) + 2\frac{x_1}{L}t - \frac{x}{L} &= 0 \\ t^2(1-2k) + 2kt - \frac{x}{L} &= 0 \end{aligned} \tag{3.4}$$

where $k = \frac{x_1}{L}$ and x are the known coordinates of the grid. An extra design variable, k, is therefore used to control the distribution of t. Knowledge of k and of the grid coordinates produces a distribution of t through the solution of eq. 3.4. Field t is used for the production of the viscosity field through eq. 3.2.

The requirement of P_i corresponding to values of viscosity is inconvenient for a problem in which the search space is unknown. Therefore, during the optimization the search space is constrained by a predefined minimum value of viscosity (ν_{min}), which helps avoiding non-physical results (i.e. negative viscosity) and an average value (ν_{ave}) to fairly compare with the homogeneous case, presented in sect. 2.6. The maximum value of viscosity is not explicitly defined. According to this parameterization, the nodal viscosity values are:

$$\nu_i = \nu_{min} + f_i(\nu_{max} - \nu_{min}) \tag{3.5}$$

where i is the ID of the cell, f_i is the non-dimensional field produced by the aforementioned procedure and ν_{max} is the maximum viscosity value, computed based on the average and minimum viscosity values as:

$$\nu_{max} = \frac{\nu_{min}(f_{ave} - 1) + \nu_{ave}}{f_{ave}} \tag{3.6}$$

$$f_{ave} = \frac{1}{A}\sum_{i=1}^{K} A_i f_i \tag{3.7}$$

where A_i is the area of cell (i), $A = \sum_{i=1}^{K} A_i$ and K the total number of cells.

The input required is summarized in the following table.

Parameters	Values	Units	Interpretation
k	[0-1]	None	Controls the final shape of the curve along the x-direction. Closer to 1 the curve moves closer to $x = L$
ν_{min}	(0-∞)	m^2/s	Minimum allowed value that the curve of kinematic viscosity may reach.
ν_{ave}	(0-∞)	m^2/s	Average value that the curve of kinematic viscosity has.
P_0	[0-1]	None	First control point. Values closer to 0 move the control point closer to ν_{min}
P_1	[0-1]	None	Second control point. Values closer to 0 move the control point closer to ν_{min}
P_2	[0-1]	None	Third control point. Values closer to 0 move the control point closer to ν_{min}

Table 3.1: *Input required by the user for the Bézier curve viscosity model.*

3.1.2 Optimization

The optimization target is to minimize the specific friction of the lubricant w.r.t. the design variables. A study -not presented herein- is carried out, prior to the optimization procedure, where it is concluded that specific friction is reduced when viscosity *decreases* along the flow. Based on this, the design variables are k, P_0 and P_2 with the intermediate control point set to $P_1 = -\sqrt{P_0 P_2}$ in order for the curve to reach the minimum value. This decision is made to minimize the search space of the optimization. The minimum value of kinematic viscosity is set to $3 \cdot 10^{-7}$ (m^2/s) corresponding to the value of water at 373 K, and the average value to $3 \cdot 10^{-6}$ (m^2/s) in order for the result to be fairly comparable to the homogeneous case of section 2.6.

The optimization procedure is set up on EASY using the following settings :

1. **Design variables**:

   The design variables are 'translated' into a binary form by 10 bits each. Using the evolutionary algorithm terminology, the chromosome of each candidate solution consists of 30 bits.

2. **Search Engine**: In order to have a faster convergence of the optimization procedure, four demes are used. Each deme is populated by 5 parents and 15

Design Variables	Minimum	Maximum	Bits
P_0	0	1	10
P_2	0	1	10
k	0.1	0.9	10

Table 3.2: *Design variables for longitudinal viscosity distribution.*

offspring, leading to a total population of 20 parents (μ) and 60 offspring (λ). The mutation probability is set to 0.02. The evolution is allowed to expand for maximum 70 generations or stops after 20 idle generations, i.e. 20 successive generations unable to locate a better solution, or 1500 evaluations based on the computational budget set (whatever comes first).

3. **Parallel Evaluations**: The optimization procedure is parallel. Thirty CPUs are used to parallelize the optimization process.

3.1.3 Results

The convergence history of the optimization is shown in fig. 3.1a. The optimized viscosity field is presented in fig. 3.1b and 3.2. The computational budget was kept at 370 CFD evaluations which was quite reasonable considering that the optimization procedure was parallelized. It is also worth noting that the evolutionary algorithm managed to locate the optimal "neighbourhood" in the first generation (60 CFD evaluations), due to the small number of design variables, after which little fluctuations around the optimized value are observed. The optimized field depicts high viscosity at the inlet and outlet of the slider, reaching the minimum value in the middle.

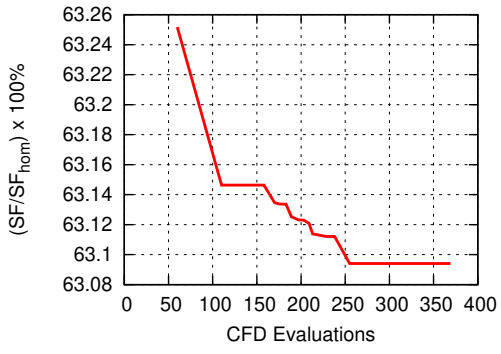

(a) *Optimization convergence. Quantity SF_{hom} is the specific friction for the homogeneous fluid with $\nu = \nu_{ave}$.*

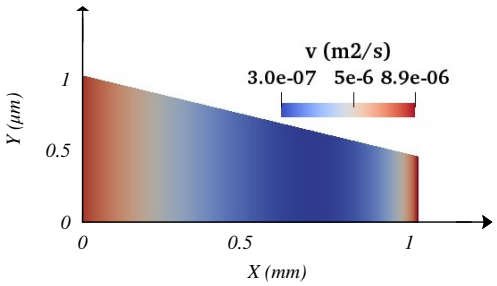

(b) *Optimized ν iso-areas (not in scale), with high viscosity at the inlet and outlet separated by a low viscosity one.*

Figure 3.1: *Optimization results.*

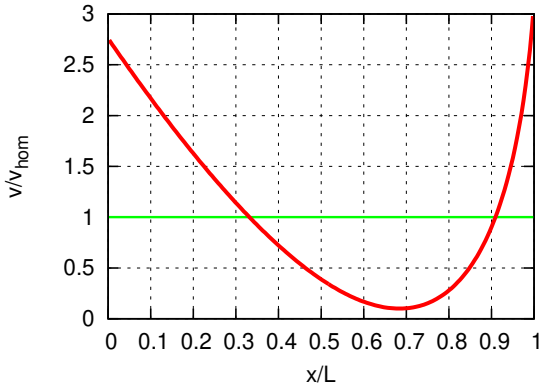

Figure 3.2: *Optimized Bézier curve describing viscosity along the slider's longitudinal direction. Quantity $\nu_{hom} = \nu_{ave}$ corresponds to the viscosity of the homogeneous case.*

Velocity and pressure results for a homogeneous fluid with $\nu = \nu_{ave}$ and the optimized inhomogeneous fluid are presented and compared. Velocity profiles are presented in fig. 3.3b at three distinct longitudinal positions. Velocity is hardly affected by the viscosity inhomogeneity. Therefore, the computation of friction depends almost exclusively on the absolute value of viscosity at each computational cell along the wall. Non-dimensional pressure profiles along the bottom wall are shown in fig. 3.3a. In contrast to velocity, pressure is significantly affected. In specific, not only the shape of the profile is changed compared to the homogeneous one but also a considerable increase is noted.

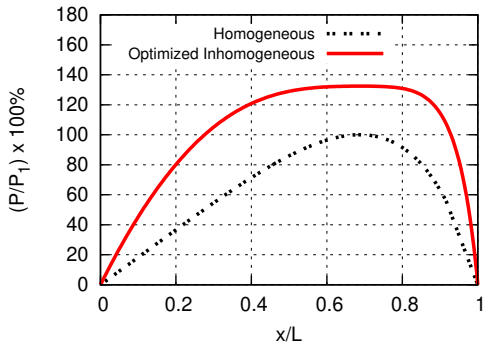

(a) *Developed non-dimensional pressure profile along the bottom wall. P_1 is the maximum developed pressure for the homogeneous fluid.*

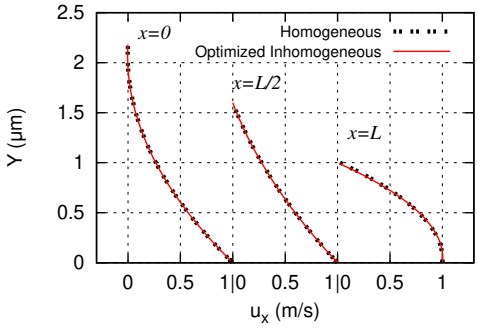

(b) *Velocity profiles along the slider's transversal direction at three axial positions. Negligible differences are observed between the homogeneous and inhomogeneous fluid results.*

Figure 3.3: *Flow fields. Comparison between the homogeneous case with $\nu = \nu_{ave}$ and the optimized case.*

Based on the above, the optimized case results in 27% SF reduction compared to the homogeneous case with $\nu = \nu_{ave}$. In specific, friction is *increased* by 1.8% and

load capacity by 62%. It is, thus, shown that the optimized longitudinal viscosity distribution does not improve friction results. However, such a distribution could potentially improve drastically the lubricant's load capacity. Overall, the optimized behaviour, as shown in this section, could potentially provide significant insight to how to "strengthen" a lubricant against extreme normal loads on the walls.

3.2 Viscosity Varying in the Transversal Direction

Nano-scale phenomena are important in an increasing number of applications, one of them being the piston ring lubrication in an internal combustion engine vehicle. These phenomena could present complexities that are nearly impossible to study, computationally or experimentally, at a finite period of time and computational power. In previous studies, inhomogeneities have been reported, through the use of MD, in the form of strong viscosity variations normal to the walls. Herein, a CFD-based optimization is carried out, seeking beneficial viscosity patterns in the transversal direction of the geometry targeting to provide valuable insight to a more extensive and computationally painful study on the nano-scale. In this section, the parameterization of ν, its optimization alongside with parametric studies are presented.

3.2.1 Parameterization

Due to the shape of the geometry, where one surface is inclined, a viscosity parameterization scheme of the form $\nu = \nu(\hat{y})$ is required, where $\hat{y}$ is the non-dimensional slider's height at each distinct position x. The viscosity transversal parameterization scheme selected consists of 11 control points piecewise linearly interpolated in each mesh cell. An appropriate viscosity model is included in the OpenFOAM environment. Through this model, the user is allowed to change the values of the control points as well as their distance leading to the creation of a viscosity field. An example case is presented in fig. 3.4 for random input from the user.

Similarly to what is presented in sect. 3.1.1, the search space is constrained by a predefined minimum value of viscosity (ν_{min}) and an average value (ν_{ave}). The maximum value is not explicitly defined. By allowing very high viscosity values, this scheme enables the continuum approach to mimic potential solidification of the fluid. The importance of this is highlighted by taking the beneficial effect of lubricative boundary tribo-films, reported in studies of ILs, into consideration.

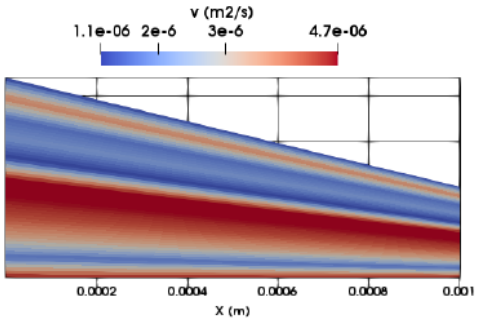

(a) *Viscosity iso-areas for example case.*

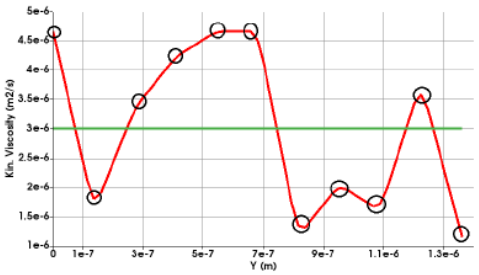

(b) *Viscosity plot across the film thickness at $x = 0.5L$. Control points are depicted with circles.*

Figure 3.4: *Example Case. Output of multiple control points-viscosity model for random input.*

The input required is summarized in table 3.3.

Parameters	Values	Units	Interpretation
ν_{min}	(0-∞)	m^2/s	Minimum allowed value that the field of viscosity may reach.
ν_{ave}	(0-∞)	m^2/s	Average value that the field of viscosity has.
$P_{1,2,...,11}$	[0-1]	None	Non-dimensional viscosity values of the control points. Values closer to 1 move the control point closer to ν_{max} .
$C_{1,2,...,11}$	[0-1]	None	Non-dimensional $\hat{y}$ values of the control points. Values closer to 1 move the control point closer to $\hat{y}_{max}$.

Table 3.3: *Input required by the user for the piecewise linear interpolation viscosity model.*

3.2.2 Optimization

The target is, once again, to minimize the specific friction. The control points are fixed in space and equidistant. Therefore, parameters $C_{1,2,...,11}$ are constant in each CFD evaluation. In specific, the values used are calculated as

$$C_{i+1} = C_i + 0.1 \quad i = 1, 2, ..., 11 \tag{3.8}$$

where $C_1 = 0$.

The minimum value of kinematic viscosity is fixed at $3 \cdot 10^{-7}(m^2/s)$ while the average value is $3 \cdot 10^{-6}(m^2/s)$. The design variables are all the parameters $P_{1,2,...,11}$.

The optimization is initialized using the following EASY settings:

1. **Design variables**:

Design Variables	Minimum	Maximum	Bits
P_1	0	1	10
P_2	0	1	10
...	0	1	10
P_{11}	0	1	10

Table 3.4: *Design variables for transversal viscosity distribution.*

2. **Metamodels**: The metamodels used are of the radial basis function (RBF) type. The minimum database entries required is 20 while the data used for the training ranged from 10 to 40.

3.2.3 Results

The convergence history of the optimization is shown in fig. 3.5a. The optimized viscosity field is presented in fig. 3.5b. Velocity and pressure results for a homogeneous fluid with $\nu = \nu_{ave}$ and the optimized inhomogeneous fluid are presented and compared. Velocity profiles are presented in fig. 3.6 at three distinct longitudinal positions alongside the shear rate at the bottom wall. Non-dimensional pressure profiles along the bottom wall are shown in fig. 3.7.

A change in the shear rate sign along the longitudinal direction is observed. Integrating this quantity along the x direction, negative contributions to friction are negated by a part of the positive ones. It is also shown that the optimized case depicts a lower absolute value of shear rate along the x direction, compared to the homogeneous case, for the 90% of the slider's length. Therefore, even though viscosity is increased near the wall, friction is greatly reduced. Additionally, an increased pressure profile is observed leading to an overall increase in load capacity. The optimized inhomogeneous case resulted in 65% SF reduction compared to the homogeneous case. In specific, the optimized case exhibits 60% friction reduction and 14% load capacity increase.

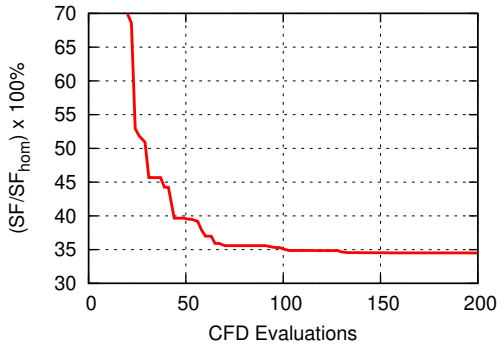

(a) *Optimization convergence. Quantity SF_{hom} is the specific friction for the homogeneous fluid with $\nu = \nu_{ave}$.*

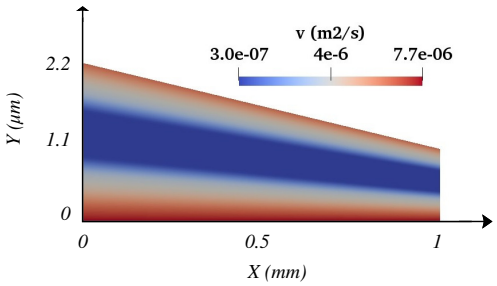

(b) *Optimized ν iso-areas (not in scale), with high viscosity layers near the solid surfaces separated by a low viscosity one.*

Figure 3.5: *Optimization results.*

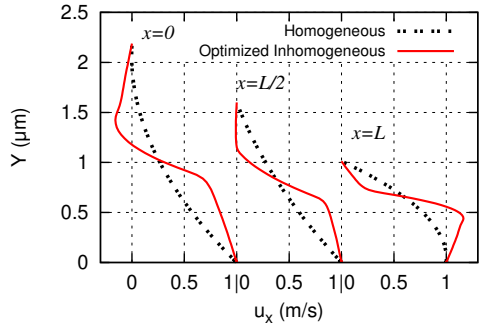

(a) *Velocity profiles along the slider's longitudinal direction. Comparison between the homogeneous and optimized inhomogeneous fluid results.*

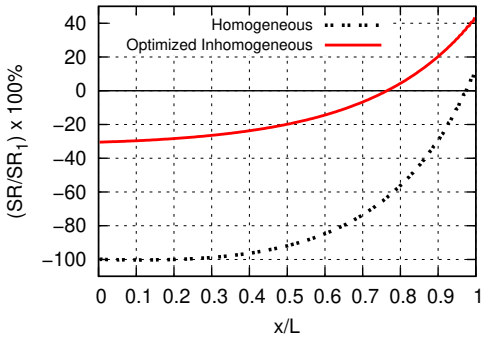

(b) *Non-dimensional shear rate along the bottom wall. SR_1 is the maximum absolute value of the shear rate for the homogeneous fluid.*

Figure 3.6: *Velocity and shear rate results.*

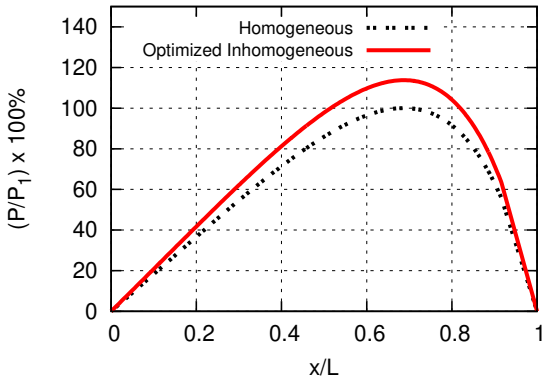

Figure 3.7: *Developed non-dimensional pressure profile along the bottom wall. P_1 is the maximum developed pressure for the homogeneous fluid. The maximum pressure of the optimized case is higher by up to 12%.*

3.2.4 Parametric Studies

In order to evaluate the sensitivity of the optimal viscosity profile to different slider configurations, parametric studies are carried out for different converging ratios (K), as in fig. 2.1, where:

$$K = \frac{h_1 - h_2}{h_2} \tag{3.9}$$

For each distinct value of K, CFD simulations are carried out for a homogeneous fluid with $\nu = \nu_{ave}$ and a fluid with the optimized viscosity profile as identified for K=1.2. The outcome of this parametric study for various K values is shown in fig. 3.8.

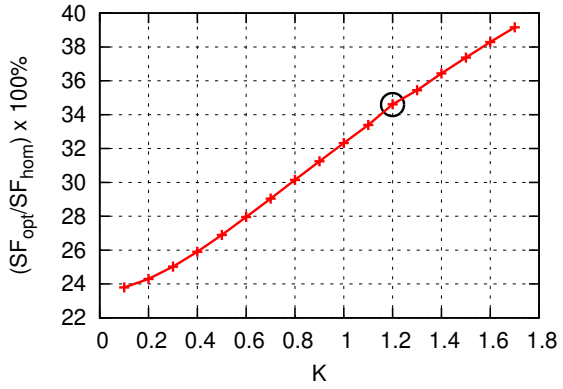

Figure 3.8: *Reduction in SF w.r.t. the homogeneous viscosity case for different converging ratios. The circled point corresponds to the converging ratio used to compute the optimized viscosity profile.*

It is worth mentioning that the percentage increase in load capacity is found to be independent of the converging ratio of the slider. Based on that, it is concluded that, as the plates tend to become parallel, the aforementioned beneficial velocity mechanism is intensified leading to a higher decrease in friction. Through this parametric study it is, therefore, shown that the optimal viscosity transversal profile, identified for a specific converging ratio, leads to beneficial friction results, compared to a conventional homogeneous lubricant, for different slider configurations. The importance of this is highlighted by taking into consideration that throughout the operation lifetime of a lubricated system, i.e. the piston rings, the geometry is bound to changes.

Figure 3.8 does not include results for parallel plates (K=0) due to the fact that, for a homogeneous fluid, the uniform pressure field obtained in such a case does not generate any extra load carrying capacity compared to the one obtained from the

reference pressure. Nevertheless, a study is carried out for a parallel plate configuration in order to identify the impact of the geometry's height on the friction results. In specific, the flows with homogeneous and optimized inhomogeneous viscosity are simulated for three different slider heights h and results are presented in table 3.5.

Table 3.5: *Friction results for parallel plates. Comparison between homogeneous and inhomogeneous fluids for different distances h between the plates.*

Plate Distance	Homogeneous	Inhomogeneous
$h = 1\ \mu m$	F_h	$0.26F_h$
$h = 0.5\ \mu m$	$2F_h$	$2 \cdot (0.26F_h)$
$h = 2\ \mu m$	$0.5F_h$	$0.5 \cdot (0.26F_h)$

The optimized ν iso-areas alongside with the velocity profiles are shown in fig. 3.9 for two parallel plates. As shown in fig. 3.9b, in the case of the parallel plates, the shear rate along the walls does not change sign. However, its absolute value is drastically decreased leading to 73% friction reduction when compared to the homogeneous case. Through this study, it is also shown that the percentage decrease of friction is independent of the distance h between the parallel plates as long as the proportion of the high viscosity zone thickness w.r.t. h is kept constant.

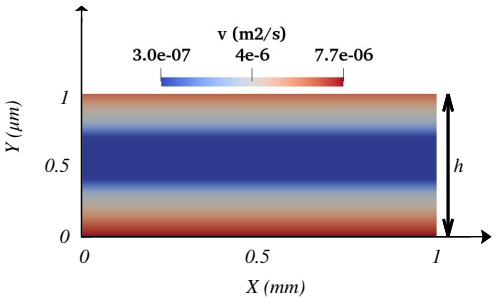

(a) *Optimized ν iso-areas for parallel plates (not in scale).*

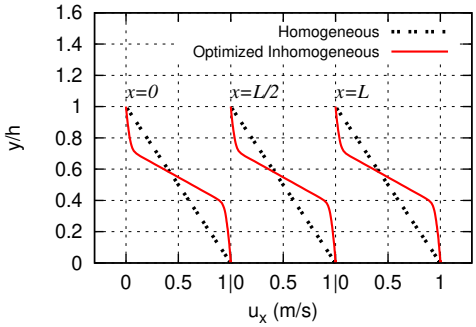

(b) *Velocity profiles along the slider's length for parallel plates. The velocity profiles remain the same for any value of distance h between the plates.*

Figure 3.9: *Parallel plates results.*

However, in practice, managing to maintain the same proportion of the liquid with high viscosity through a large gap would be a difficult task, in terms of controlling the lubricant properties far from the lubricated walls. For this reason, a second study of parallel plates with varying distance h is carried out, this time with a fixed thickness of the high viscosity layer. In specific, CFD simulations are carried out in which the high viscosity zones correspond to an absolute value of 0.4 μm thickness normal to the walls and viscosity value equal to 80% of the maximum value observed

in the optimized case. The low viscosity value is calculated for each case based on the slider's height in order for the inhomogeneous simulation to be fairly comparable with a homogeneous case with $\nu = \nu_{ave}$.

This study shows, fig. 3.10a, a negligible impact of viscosity inhomogeneity in case of large gaps, where the bulk properties of the lubricant play the main role. Also, for computational efficiency, even if it can be assumed that viscosity inhomogeneity does occur near the walls, it can be safely ignored when the total height of the slider is significantly larger than the thickness of the high viscosity zone. However, when the thickness of the high viscosity zone becomes significant as a proportion of the total height (e.g. 8% for the 10 μm case), then a quantifiable benefit can be observed and thus such inhomogeneities cannot be ignored. Corresponding velocity profiles are shown in fig. 3.10b for different slider heights. It is observed that when the gap is significantly larger than the high viscosity zone, the velocity of the homogeneous and inhomogeneous cases are practically the same.

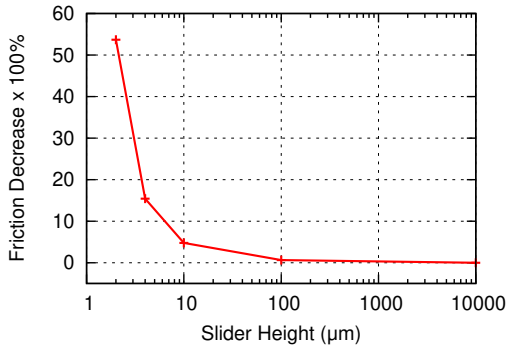

(a) *Friction results for varying distances h between the parallel plates. Friction decrease corresponds to* $\frac{F_{hom}-F_{inh}}{F_{hom}}$*, where* F_{hom} *and* F_{inh} *are the absolute values of friction for the homogeneous and inhomogeneous viscosity cases, respectively.*

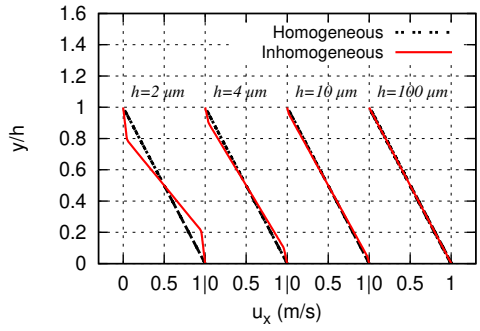

(b) *Velocity profiles for varying distance h between the parallel plates. As the distance increases, while the high viscosity zone thickness remains the same, the inhomogeneous and homogeneous case do not exhibit any observable difference.*

Figure 3.10: *Results for parametric study of varying h and constant high viscosity zone thickness.*

Chapter 4

Anisotropic Fluids

In material science and engineering, anisotropy is a material's directional dependence of a physical property. One such material is liquid crystals. The anisotropic behaviour of liquid crystals is due to the elongated shape of the molecules. The physical properties of the molecules are different when measured parallel or perpendicular to their length. Residual alignment of the rods in the fluid leads to anisotropic bulk properties. This residual alignment occurs as a result of preferential packing arrangements and electrostatic interactions between molecules that are most favourable (lowest in energy) in aligned configurations.

In this chapter, a model of an anisotropic incompressible viscous fluid is presented. The model is implemented in the OpenFOAM environment targeting at simulating the aforementioned rheological behaviour in the continuum domain. In specific, this study tries to identify the effect, of inherently anisotropic molecular systems, on lubrication performance through a continuum approach.

4.1 Anisotropic Viscous-Stress Tensor

Adopting the approach to the description of inherently anisotropic homogeneous continua that was proposed by Oldroyd [31], a simple linear model of an anisotropic incompressible viscous fluid whose local structure is represented by a physical constant tensor, is presented.

The viscous stress is due to the relative motion on the continuum scale and therefore

depends on velocity gradients

$$\frac{\partial u_i}{\partial x_j}, \frac{\partial^2 u_i}{\partial x_j \partial x_k} ....$$

The relation between the viscous stress (τ_{ij}) and the velocity gradient ($\frac{\partial u_i}{\partial x_j}$) is considered linear. For second-rank tensors, the most general linear relation is:

$$\tau_{ij} = C_{ijlm} \frac{\partial u_l}{\partial x_m} \tag{4.1}$$

where C_{ijlm} is a coefficient tensor of rank four. In principle, there are $3^4 = 81$ coefficients for a three-dimensional approach and decrease to 16 for a two-dimensional. It can be shown that, in an isotropic fluid, the fourth-rank tensor is of the following form:

$$C_{ijlm} = \lambda \delta_{ij} \delta_{lm} + \mu(\delta_{il}\delta_{jm} + \delta_{im}\delta_{jl}) \tag{4.2}$$

Therefore 81 coefficients reduce to two, λ and μ and are called viscosity coefficients. By this definition, the viscous stress tensor is:

$$\tau_{ij} = \mu\Big(\frac{\partial u_i}{\partial x_j} + \frac{\partial u_j}{\partial x_i}\Big) + \lambda \frac{\partial u_l}{\partial x_l} \delta_{ij} \tag{4.3}$$

and for an incompressible fluid, w.r.t the continuity equation, reduces to:

$$\tau_{ij} = \nu\Big(\frac{\partial u_i}{\partial x_j} + \frac{\partial u_j}{\partial x_i}\Big) \tag{4.4}$$

In the proposed model, the definition of the isotropic viscous stress tensor 4.4 is altered in order for this to be in accordance with 4.1 and is denoted as τ'_{ij}.

$$\begin{aligned} \tau'_{ij} &= C_{ijlm} \frac{\partial u_l}{\partial x_m} \\ \tau'_{ij} &= (c_{ijlm} + \nu_{ijlm}) \frac{\partial u_l}{\partial x_m} \end{aligned} \tag{4.5}$$

where

$$c_{ijlm} = \nu_c(\delta_{il}\delta_{jm} + \delta_{im}\delta_{jl})$$

and ν_c corresponds to a bulk kinematic viscosity. The decision of 'splitting' tensor C_{ijlm} into c_{ijlm} and ν_{ijlm} is made due to the fact that even in an anisotropic approach, the fluid is expected to correspond to a bulk viscosity value, expressed by c_{ijlm}, which due to anisotropy is to illustrate minor differences depending on the orientation, expressed by ν_{ijlm}. It also provides the study with the ability of fairly comparing the fluid under investigation with an isotropic one with the same bulk viscosity value.

From equation 4.5, the sum of the components c_{ijlm} and ν_{ijlm} correspond to a physical constant that one would naturally call viscosity tensor. Component c_{ijlm} depicts the isotropic term of the tensor while ν_{ijlm} the term under evaluation.

This description leads to an altered momentum equation:

$$\begin{aligned}
u_j\frac{\partial u_i}{\partial x_j} - \frac{\partial}{\partial x_j}\Big[\big[\nu_c(\delta_{il}\delta_{jm} + \delta_{im}\delta_{jl}) + \nu_{ijlm}\big]\frac{\partial u_l}{\partial x_m}\Big] + \frac{\partial p}{\partial x_i} &= 0 \\
u_j\frac{\partial u_i}{\partial x_j} - \frac{\partial}{\partial x_j}\Big[\nu_c\Big(\frac{\partial u_i}{\partial x_j} + \frac{\partial u_j}{\partial x_i}\Big) + A_{ij}\Big] + \frac{\partial p}{\partial x_i} &= 0 \\
u_j\frac{\partial u_i}{\partial x_j} - \frac{\partial}{\partial x_j}\Big[\nu_c\Big(\frac{\partial u_i}{\partial x_j} + \frac{\partial u_j}{\partial x_i}\Big)\Big] + \frac{\partial p}{\partial x_i} - \frac{\partial}{\partial x_j}\Big(A_{ij}\Big) &= 0, \quad i,j = 1,2
\end{aligned} \tag{4.6}$$

where $A_{ij} = \nu_{ijlm}\frac{\partial u_l}{\partial x_m}$ and

$$\begin{aligned}
(\delta_{il}\delta_{jm} + \delta_{im}\delta_{jl})\frac{\partial u_l}{\partial x_m} &= \delta_{il}(\delta_{jm}\frac{\partial u_l}{\partial x_m}) + \delta_{im}(\delta_{jl}\frac{\partial u_l}{\partial x_m}) \\
&= \delta_{il}\frac{\partial u_l}{\partial x_j} + \delta_{im}\frac{\partial u_j}{\partial x_m} \\
&= \frac{\partial u_i}{\partial x_j} + \frac{\partial u_j}{\partial x_i} = 2\epsilon_{ij}
\end{aligned} \tag{4.7}$$

where ϵ_{ij} is the rate of strain (strain-rate) tensor.

While this model is programmed and included in the OpenFOAM environment in its most general form, as presented in equation 4.6, some assumptions are made for its applications.

Assuming that there are no finite body couples per unit mass in the fluid, the stress tensor is symmetric and

$$\nu_{ijlm} = \nu_{jilm} \tag{4.8}$$

4.2 Developed SimpleAnisoFoam

The set of equations to be solved is the continuity equation for an incompressible fluid and the momentum equation 4.6. The formulation of equation 4.6 leads to a purely isotropic part (corresponding to the classic N-S equations) and an anisotropic term $\left(\frac{\partial}{\partial x_j}(A_{ij})\right)$. Thus, the implementation of the model in the OpenFOAM environment is realized through the alteration of the already existent *simpleFoam* solver. The anisotropic term is included explicitly into the solution process, meaning that its values at iteration n are expressed, only, as function of values obtained at $n-1$.

The input required is the same as with *simpleFoam*, with the addition of four, rank two, non-dimensional tensors (C^{11}_{lm}, C^{12}_{lm}, C^{21}_{lm}, C^{22}_{lm}) that are called *constructing tensors*. As the name suggests, these tensors are required by the user for the construction of the final ν_{ijlm}. The constructing tensors are multiplied with the bulk value of kinematic viscosity ν_c as used in equation 4.6.

The code proceeds to compute the double inner product of the four tensors with the gradients of velocity on each iteration of SIMPLE

$$A_{ij} = C^{ij}_{lm} : \frac{\partial u_l}{\partial x_m} \quad \text{with i,j,l,m} = 1, 2$$

For instance, term A_{11} is calculated as

$$A_{11} = C^{11}_{11}\frac{\partial u_1}{\partial x_1} + C^{11}_{12}\frac{\partial u_1}{\partial x_2} + C^{11}_{21}\frac{\partial u_2}{\partial x_1} + C^{11}_{22}\frac{\partial u_2}{\partial x_2} \tag{4.9}$$

where $C^{11}_{11}, C^{11}_{12}, ...$ are the terms of the constructing tensor C^{11}_{lm}. The computed term is then added to the momentum equation as described in eq. 4.6 and the algorithm continues until convergence.

4.3 Couette and Poiseuille Flow

Prior to any optimization, an investigation of the anisotropic model on the parallel plate geometry is carried out in order to evaluate the validity of the model on simple flows. In specific, the geometry is depicted by two parallel plates of total height $h = 2\ \mu m$ and the boundary conditions are set to express a Couette and a Poiseuille flow, respectively. Both flows are expressed by simple analytical solutions and are, thus, used to obtain new analytical expressions based on eq. 4.6. Based on these expressions -their derivation is shown below- the model is used to evaluate whether the analytical results are the same with the simulation ones.

As regards the Couette flow, the boundary conditions are the same to the ones used in the previous chapters of this thesis. The velocity profile is considered to be fully developed and thus

$$\frac{\partial u_x}{\partial x} = 0$$

Based on this and taking into consideration the continuity equation, it is also true that

$$\frac{\partial u_y}{\partial y} = 0$$

Since $\frac{\partial u_y}{\partial y} = 0$ and $u_y|_{wall} = 0$, therefore $u_y = 0$ in the whole domain. Based on the above, the convection term of the N-S equations is zero and the momentum equation as described by eq. 4.6 can be written:

$$\frac{\partial}{\partial x_j}\Big[\nu_c\Big(\frac{\partial u_i}{\partial x_j} + \frac{\partial u_j}{\partial x_i}\Big)\Big] + \frac{\partial}{\partial x_j}\Big(A_{ij}\Big) = \frac{\partial p}{\partial x_i} \tag{4.10}$$

In the Couette flow, it is assumed that there is no pressure gradient in the longitudinal direction of the flow and thus $\frac{\partial p}{\partial x} = 0$. Also, all gradients of velocity are zero except $\frac{\partial u_x}{\partial y}$ which leads to $\frac{\partial p}{\partial y} = 0$. Therefore, eq. 4.10 can be written as:

$$\frac{\partial}{\partial y}\left[\nu_c \frac{\partial u_x}{\partial y}\right] + \frac{\partial}{\partial y} A_{xy} = 0 \tag{4.11}$$
$$\frac{\partial}{\partial y}\left[(\nu_c + \nu_{xyxy})\frac{\partial u_x}{\partial y}\right] = 0$$
$$(\nu_c + \nu_{xyxy})\frac{\partial^2 u_x}{\partial y^2} = 0$$

It is, thus, shown that by implementing an anisotropic term in eq. 4.6 for a Couette flow, the velocity profile does not change compared to the isotropic. Nevertheless, simulations are carried out for an isotropic and an anisotropic case, respectively. In specific, in the isotropic case $A_{ij} = 0$ and $\nu_c = 3 \cdot 10^{-6}\ \frac{m^2}{s}$. As for the anisotropic case, ν_c remains the same and the constructing tensor C^{12}_{lm} is activated with $C^{12}_{12} = 1$ and the rest of its terms remaining zero. The resulted velocity profile is depicted in fig. 4.1. It is shown, therefore, that for both cases the velocity profile is the same.

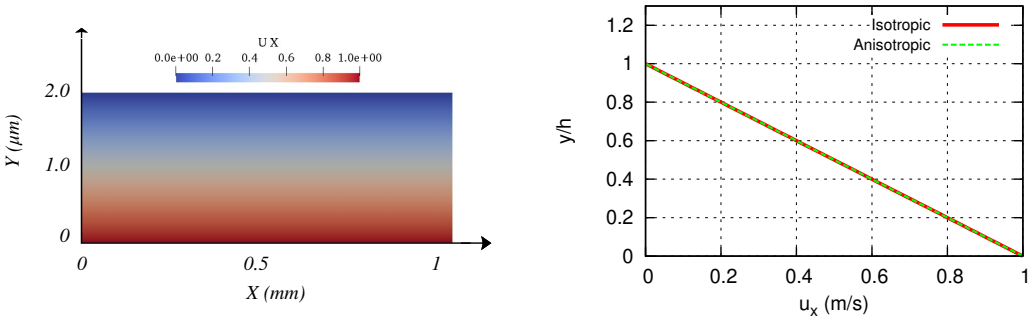

(a) *Velocity iso-areas for both isotropic and anisotropic case (not in scale).*

(b) *Velocity profile along the film thickness.*

Figure 4.1: *Velocity results. Comparison between the isotropic and anisotropic case.*

However, in order to be consistent to the description of eq. 4.6, friction computation on the walls is altered to include the tangential to the wall force coefficient of A_{ij}. Therefore, the programmed post-processor is enhanced with

$$F = \int_0^L \tau'_{xy} dx = \int_0^L \left[\nu_c \frac{\partial u_x}{\partial y} + A_{xy}\right] dx \tag{4.12}$$

Based on this, the computed friction for the anisotropic case is doubled compared to the one of the isotropic case.

As concerns the Poiseuille flow, the geometry of the problem remains the same but the boundary conditions change. In specific, for the velocity no-slip is assumed at the

still walls and a zero Neumann at the inlet and outlet. For the pressure, a constant Dirichlet P_1 is applied in the inlet and a constant P_2 at the outlet, with $P_1 > P_2$. At the walls, a zero Neumann condition is applied for the pressure. Following the same assumptions as for the Couette flow, it can be shown that the governing equations simplify to:

$$\begin{aligned} \frac{\partial p}{\partial x} =& \frac{\partial}{\partial y}(\nu_c \frac{\partial u_x}{\partial y}) + \frac{\partial}{\partial y}(A_{xy}) \\ \frac{\partial p}{\partial y} =& 0 \end{aligned} \tag{4.13}$$

It can be assumed that the quantity $\frac{\partial p}{\partial x} = -\frac{\Delta p}{L}$, where $\Delta p = P_1 - P_2$ and L is the total length of the geometry. Also, similar to the Couette flow it can be assumed that the only "rational" term of anisotropy is ν_{xyxy} and thus:

$$-\frac{\Delta p}{L} = (\nu_c + \nu_{xyxy})\frac{\partial^2 u_x}{\partial y} \tag{4.14}$$

Since the flow is considered fully developed, the partial derivative can be changed to an ordinary one and, by integrating twice, eq. 4.14 the velocity profile along the film thickness can be expressed as:

$$u_x(y) = -\frac{\Delta p}{2L(\nu_c + \nu_{xyxy})}y^2 + C_1 y + C_2 \tag{4.15}$$

and by applying the boundary conditions:

$$u_x(y) = \frac{\Delta p}{2L(\nu_c + \nu_{xyxy})}(h^2 - y^2) \tag{4.16}$$

where h is the total height of the geometry. At this point, it is reminded that in the programmed model, terms of anisotropy are included in proportion to the bulk viscosity value ν_c. Therefore, eq. 4.16 can be written as:

$$u_x(y) = \frac{\Delta p}{2L(1 + k)\nu_c}(h^2 - y^2) \tag{4.17}$$

where $\nu_{xyxy} = k\nu_c$. In order to evaluate the model based on the previous analysis, two simulations of isotropic and anisotropic fluids, respectively, are carried out. In

specific, for the isotropic case $k = 0$ while for the anisotropic one $k = 1$. The velocity results are presented in figs. 4.2 and 4.3. It can be seen that the anisotropic case exhibits half the velocity in each computational cell compared to the isotropic one, as expected from eq. 4.17. However, based on the new calculation 4.12, friction does not exhibit any change.

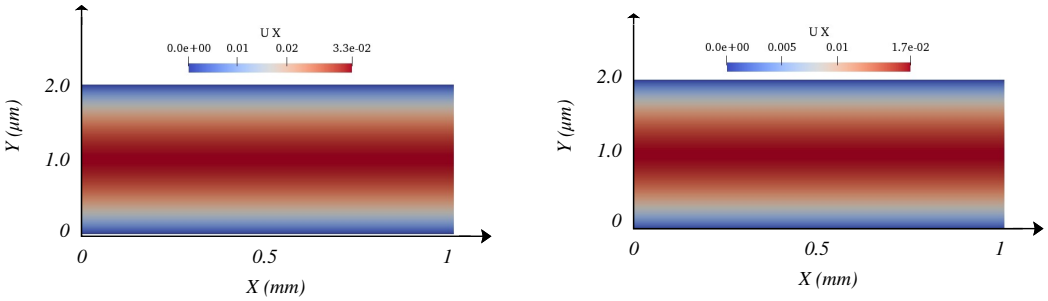

(a) *Velocity iso-areas for the isotropic case with $k = 0$ (not in scale).*

(b) *Velocity iso-areas for the anisotropic case with $k = 1$ (not in scale).*

Figure 4.2: *Velocity iso-areas. Comparison between the isotropic and anisotropic case.*

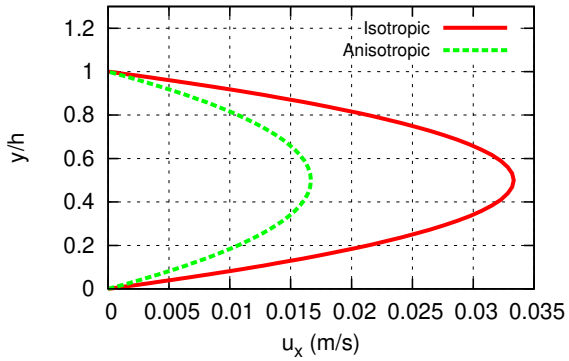

Figure 4.3: *Velocity profiles for Poiseuille flow of an isotropic and an anisotropic fluid.*

Based on the above studies, the model is deemed to be valid and an optimization process can commence.

4.4 Optimization

The optimization target is to minimize the specific friction w.r.t. the values of the constructing tensors. By changing the values of these tensors, this study enables

the investigation of the impact of anisotropy, in the form of tensorial viscosity, to lubrication performance parameters. However, instead of setting one optimization targeting to minimize specific friction, two are used. One targets at minimizing friction and one at maximizing load capacity (the computation of load capacity remains the same and the impact of anisotropy is investigated solely through the pressure field). The geometry under examination is that of the converging hydrodynamic slider (fig. 2.1).

The bulk viscosity is set to $\nu_c = 3 \cdot 10^{-6} \frac{m^2}{s}$, in order to compare with the isotropic case. Interest is given to the impact of the non-diagonal terms of τ'_{xy} and thus terms of C^{12}_{lm} and C^{21}_{lm} are used as design variables, while $C^{11}_{lm} = C^{22}_{lm} = 0$. In specific, all terms C^{ij}_{lm} with $i \neq j$ and $l \neq m$ are selected. Based on the assumption 4.8 the design variables are 2, C^{12}_{12} and C^{12}_{21} with $C^{12}_{12} = C^{21}_{12}$ and $C^{12}_{21} = C^{21}_{21}$. For the sake of simplicity, the first design variable is denoted as A and the second one as B. Therefore, the viscous stress tensor can be written as

$$\tau'_{ij} = \begin{bmatrix} 2\nu_c \frac{\partial^2 u_x}{\partial x^2} & \nu_c(1+A)\frac{\partial u_x}{\partial y} + \nu_c(1+B)\frac{\partial u_y}{\partial x} \\ \nu_c(1+A)\frac{\partial u_x}{\partial y} + \nu_c(1+B)\frac{\partial u_y}{\partial x} & 2\nu_c \frac{\partial^2 u_y}{\partial y^2} \end{bmatrix} \tag{4.18}$$

The optimizations is carried out by the following EASY settings:

1. **Design variables**:

Design Variables	Minimum	Maximum	Bits
A	-0.5	1.5	10
B	-0.5	1.5	10

Table 4.1: *Design variables for tensorial viscosity.*

The design variables are 'translated' into a binary form by 10 bits each. The range of design variables, illustrated in table 4.1, is decided based on the fact that minor changes to the bulk viscosity are expected on a molecular system. Negative values are also allowed since, as shown in 4.18, they don't correspond to unphysical negative diffusion.

4.4.1 Results

The convergence history for the optimization targeting at minimum friction and the one targeting at maximum load capacity are presented in fig. 4.4a & 4.4b, respectively. Both optimizations computed the optimal solution in only a few evaluations due to the small number of design variables (2).

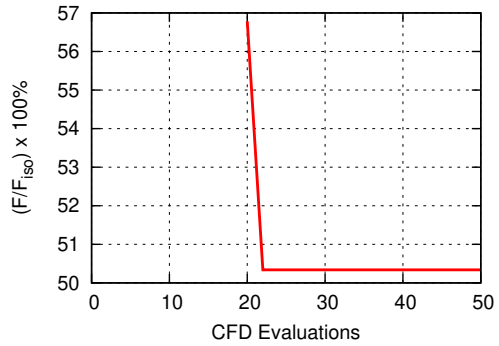

(a) *Convergence history for the optimization targeting minimum friction. Quantity F_{iso} corresponds to the computed value of friction for the isotropic fluid.*

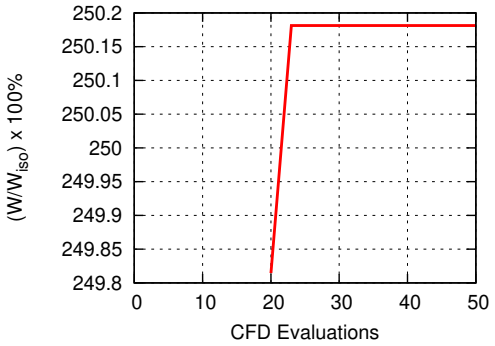

(b) *Convergence history for the optimization targeting to maximum load capacity. Quantity W_{iso} corresponds to the computed value of load capacity for the isotropic fluid.*

In specific, the design variables of the optimization targeting minimum friction both reached their minimum allowed values $A = B = -0.5$. On the other hand, the one targeting maximum load capacity had $A = 1.5$ and $B = -0.5$ in the optimal solution. Bearing in mind that B is involved in the $\frac{\partial u_y}{\partial x}$ contribution of the viscous stress tensor, it is significantly less important compared to A.

However, as regards the friction reduction case, 50% load capacity reduction is observed as well. Similarly, in the maximized load capacity case, friction is increased by 250%. Therefore, no case managed to locate an optimized result for specific friction. Nevertheless, it is shown that by implementing anisotropic properties on the fluid, which in turn could result in a different design on a molecular basis, one can manipulate the friction and load capacity of a potential lubricant.

In conclusion, through this preliminary study it is shown that an inherently anisotropic fluid cannot benefit lubrication, in terms of specific friction reduction. However, it is expected that by coupling anisotropy with inhomogeneity, by assuming that the values of the *constructing tensors* are spatial dependent, one can achieve significantly optimized results. Relevant studies have been made on the nano-scale for liquid crystals showing favourable friction results [32].

Chapter 5

Nano-scale Study

Continuum methods, while capable of efficiently solving macroscopic problems, cannot resolve features and flow patterns at the nano-scale, due to the breakdown of the continuum assumption. On the other hand, atomistic simulations can provide fundamental insights in the fluid behaviour but at a high computational cost. In this chapter, a brief description of the simulation technique of molecular dynamics (MD), alongside with applications set on an attempt to bridge the macro-scale with the nano-scale, are presented.

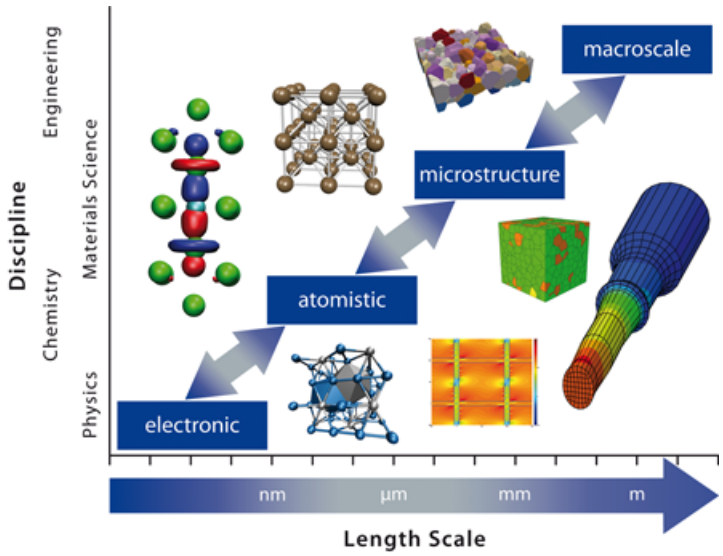

Figure 5.1: *The interdisciplinary multi-scale material modeling framework [33].*

Traditionally different disciplines focus on different length scales. Multi-scale modeling of materials across the length scales requires overcoming the borders between the disciplines for a seamless integration of the models at different length scales into

one coherent multi-scale modeling framework.

5.1 Molecular Dynamics

The idea of molecular dynamics (MD) [34] is that of numerically integrating the classical equations of motion to generate a trajectory of a system with N particles in time. The particles are characterized by 3N coordinates, namely positions and momenta in a three dimensional volume space. The Newton's equations for a particle i subjected to a force f_i at time t are:

$$\frac{d^2\vec{r_i}}{dt^2} = \frac{\vec{f_i}(\vec{r_1}, \vec{r_2}, ..., \vec{v_1}, \vec{v_2}, ...)}{m_i} \tag{5.1}$$

where the force depends on the particle positions and eventually velocities.

A typical MD program follows this scheme:

1. At time $t = 0$, initialize the system by choosing positions and velocities of the particles. Choose also a value of Δt, the time step used in the numerical integration of the equations of motion.
2. Compute the forces on all particles based on their potential energy.
3. Integrate the Newton's equations of motion using an appropriate integration scheme. Update positions and velocities of particles at time $t + \Delta t$.
4. Go back to step 2.

Differently from the stochastic Monte Carlo simulations, MD is a deterministic method. Given an initial condition, a MD program always generates the same trajectory in phase space.
Physical quantities are computed from time averages along the trajectories. Let A be a quantity depending on positions and velocities such as

$$A(t) = A(\vec{r_1}(t), ...\vec{r_N}(t), \vec{v_1}(t), ...\vec{v_N}(t))$$

Then, its average value is defined as

$$\langle A \rangle = \frac{1}{N} \sum_{n=0}^{N-1} A(t_0 + n\Delta t) \tag{5.2}$$

where t_0 is an initial time. Typically, a physical quantity is characterized by some

relaxation time τ_A, which is the time one has to wait until A reaches an average equilibrium value. If one is interested in equilibrium quantities, it is safer to take averages starting from a given time $t_0 > \tau_A$.

5.1.1 Integration schemes

The simplest integration scheme and also the mostly used is the so-called Verlet's algorithm. Through a Taylor expansion up to the fourth order for position

$$\vec{r_i}(t + \Delta t) = \vec{r_i}(t) + \vec{v_i}(t)\Delta t + \frac{\vec{a_i}(t)}{2}\Delta t^2 + \frac{\vec{g_i}(t)}{6}\Delta t^3 + O(\Delta t^4) \tag{5.3}$$

$$\vec{r_i}(t - \Delta t) = \vec{r_i}(t) - \vec{v_i}(t)\Delta t + \frac{\vec{a_i}(t)}{2}\Delta t^2 - \frac{\vec{g_i}(t)}{6}\Delta t^3 + O(\Delta t^4) \tag{5.4}$$

where $\vec{v_i} = \frac{d\vec{r_i}}{dt}$, $\vec{a_i} = \frac{d^2\vec{r_i}}{dt^2}$ and $\vec{g_i} = \frac{d^3\vec{r_i}}{dt^3}$. By summing up eqs. 5.3 & 5.4, one arrives at the Verlet algorithm:

$$\vec{r_i}(t + \Delta t) = 2\vec{r_i}(t) - \vec{r_i}(t - \Delta t) + \vec{a_i}(t)\Delta t^2 + O(\Delta t^4) \tag{5.5}$$

Therefore, through this equation, positions are computed accurate up to Δt^4. The velocities are not explicitly calculated, but they can be derived from the knowledge of the trajectory as

$$\vec{v_i}(t) = \frac{\vec{r_i}(t + \Delta t) - \vec{r_i}(t - \Delta t)}{2\Delta t} + O(\Delta t^2) \tag{5.6}$$

which is accurate only to the order Δt^2. Hence, quantities depending on the velocities, as the total kinetic energies are not accurately determined. As shown from eq. 5.5, the position of the particles at time step $t + \Delta t$ depends on positions at times t and $t - \Delta t$. Therefore, initial conditions in which the $t = 0$ positions and velocities are given, are not enough. The problem is solved by approximating

$$\vec{r_i}(\Delta t) \approx \vec{r_i}(0) + \vec{v_i}(0)\Delta t + \frac{\vec{a_i}(0)}{2}\Delta t^2 \tag{5.7}$$

From it, forces can be computed, hence $\vec{a_i}(\Delta t)$ and then apply iteratively eq. 5.5.

5.1.2 Velocity Verlet Algorithm

An alternative and much better integration scheme, where positions and velocities are simultaneously updated, is the so-called Velocity Verlet algorithm. It can be expressed by the following two equations

$$\vec{r_i}(t+\Delta t) = \vec{r_i}(t) + \vec{v_i}(t)\Delta t + \frac{\vec{a_i}(t)}{2}\Delta t^2 + O(\Delta t^4) \tag{5.8}$$

$$\vec{v_i}(t+\Delta t) = \vec{v_i}(t) + \frac{\vec{a_i}(t+\Delta t) + \vec{a_i}(t)}{2}\Delta t \tag{5.9}$$

An important feature of the Verlet and Velocity Verlet algorithms is that they are fully time reversal: eq. 5.5 remains invariant by interchanging $\Delta t \to -\Delta t$. Another property of the Velocity Verlet algorithm is that it is a symplectic integrator[1].

What is impractical of the Velocity Verlet algorithm as given by eqs. 5.8 & 5.9 is that it requires storage of accelerations at two different time steps. An implementation avoiding this is the following

1. Given $\vec{r_i}(t)$, $\vec{v_i}(t)$ and $\vec{a_i}(t)$ update the positions through eq. 5.8.
2. Calculate the velocities at an intermediate time step

$$\vec{v_i}(t+\frac{\Delta t}{2}) = \vec{v_i}(t) + \frac{1}{2}\vec{a_i}(t)\Delta t \tag{5.10}$$

3. From the positions at $t+\Delta t$ calculate the forces and hence accelerations. If forces are derived from a velocity independent potential V then

$$\vec{a_i}(t+\Delta t) = -\frac{1}{m} \bigtriangledown V_i(\vec{r_1}(t+\Delta t)...\vec{r_N}(t+\Delta t)) \tag{5.11}$$

4. Update the velocities to

$$\vec{v_i}(t+\Delta t) = \vec{v_i}(t+\frac{\Delta t}{2}) + \frac{1}{2}\vec{a_i}(t+\Delta t)\Delta t \tag{5.12}$$

The aforementioned algorithm is identical to eqs. 5.8 and 5.9. However the latter equation is implemented in two steps. This way memory requirements are decreased since there is no need to store data at two different time steps. For a system of N

[1]Such algorithms have the property that their trajectories conserve exactly "pseudo-energy" which differs from the true energy by a small amount (vanishing as $\Delta t \to 0$).

particles in three dimensions, one needs $9N$ memory locations: $3N$ for positions, velocities and accelerations, respectively.

5.1.3 Initialization

A MD simulation begins by giving a set of initial positions and velocities to the particles. The positions can be initialized by putting the particles in some lattice points or through the use of a random number generator. The velocities can be selected from some distribution. One imposes the condition that the total momentum vanishes. So, if the initial selection yields

$$\vec{P}_{TOT} = \sum_{i=1}^{N} m_i \vec{v_i}(0) \neq 0 \tag{5.13}$$

then

$$\vec{v_i}(0) \rightarrow \vec{v_i}(0) - \frac{\vec{P}_{TOT}}{m_i N} \tag{5.14}$$

The most important test that needs to be made to check the stability of the MD simulation is the conservation of the total energy.

5.1.4 Lennard-Jones Potential

A widely studied system is the Lennard-Jones (LJ) fluid, which is defined by the potential

$$V_{LJ}(r) = 4\epsilon\Big[(\frac{\sigma}{r})^{12} - (\frac{\sigma}{r})^{6}\Big] \tag{5.15}$$

where σ is the zero potential distance and ϵ the well depth. This potential is illustrated in fig. 5.2.

The potential has a short range repulsive term ($\sim \frac{1}{r^{12}}$) and a long range attractive term ($\sim \frac{1}{r^{6}}$). The origin of the attractive force is quantum-mechanical and due to fluctuating dipoles (Van der Waals interactions). The choice of a power $\sim \frac{1}{r^{12}}$ at short distances has no theoretical justification and is chosen exclusively because of ease of computation. Its origin is related to the Pauli principle, which states that when the electronic clouds surrounding the atoms start to overlap, the energy of the system increases abruptly.

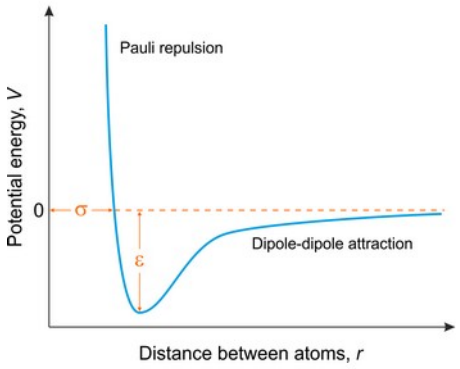

Figure 5.2: *The Lennard-Jones pair potential.*

In this thesis, all particle interactions are described through the use of the LJ potential. There are other intramolecular interactions such as electrostatic interactions or molecular ones but they are not considered herein to ease the computational process.

5.2 Parallel Plates Model

In the previous chapters, an extensive study is presented in order to determine the optimal distribution of viscosity in a fluid's flow through a converging hydrodynamic slider. On an attempt to bridge the information provided from the macro-scale with the nano-scale, coarse grain molecular dynamics simulations [2] are set and results are presented and discussed.

Through the atomistic approach, optimal patterns of the macro-scale are sought on the nano-scale, in order to verify their beneficial behaviour on lubrication. An exact representation is, however, impossible due to inherent restrictions of the modeling process. Such restrictions are:

1. Necessity of periodic boundary condition at the inlet and outlet of the simulation box, restricts the representation of a longitudinal inhomogeneous viscosity flow.

2. Dimensions are greatly reduced.

Based on this, a transversal viscosity inhomogeneity is sought in accordance with sect. 3.2. The 2D geometry used to model the shear flows involves two parallel plates

[2] Coarse-grained modeling, aim at simulating the behaviour of complex systems using a simplified representation. In this models, molecules are represented by 'pseudo-atoms' approximating groups of atoms. Much longer simulation times can be studied. [35]

and the space between them. The top plate is forced to remain stationary while the bottom plate is moving with a constant velocity $\vec{V} = (V_x, 0)$. The simulation box is $\sim$ 160 Å long in the x- and $\sim$ 80 Å in the y- direction. The fluid is kept at a temperature of T=303 K by means of a Nosé-Hoover NVT thermostat. Finally, periodic conditions are applied at the left and right boundary, ensuring that particles can interact across the boundary, and non-periodic ones along the y- direction, as the plates are artificially forced to remain at their starting y-position.

5.2.1 Bulk fluid properties

Driven by the findings of the continuum study, sect. 3.2 a reproduction of three bulk fluids with different viscosities is sought. In specific, one particle type is used to reproduce the homogeneous fluid and two particle types for the optimized inhomogeneous one. The particle type describing the homogeneous fluid is denoted by (I) while the ones describing the inhomogeneous one by (H) and (L). The LJ parameters, describing each particle interaction, are tuned accordingly in order for particles (H), (L) and (I) to have high, low and intermediate viscosity values, respectively.

For each particle description, a viscosity computation using the Green-Kubo relation is made. Temperature is set to 303 K by means of a Nosé-Hoover NVT thermostat. A total of 1600 particles are randomly placed on a simulation box with dimensions as described above. Due to the stochasticity of the procedure, 5 independent trajectories are simulated for each fluid. The LJ tuned parameters for each particle type are shown in table 5.1. The averaged viscosity and density for each fluid, containing solely particles of one type, are shown in table 5.2.

Table 5.1: *List of LJ parameters for particle types (I), (H) and (L). Parameters correspond to* $E = 0.250$ *eV,* $\Sigma = 2.5$ *Å.*

Pair	ϵ	σ	R_c
(I)-(I)	E	Σ	4Σ
(H)-(H)	$1.2E$	Σ	4Σ
(L)-(L)	$0.8E$	Σ	4Σ

In order to be consistent with the shear flow simulations, all viscosity computations are performed in a 2D simulation box, with the aforementioned dimensions. The simulation is periodic in both directions and no walls are included. Results presented in table 5.2 are computed by assuming a nominal depth of 1 Å. Each particle molar mass is set equal to 18 $\frac{g}{mol}$.

Table 5.2: *Statistically averaged viscosity and density results based on the Green-Kubo computations for three bulk fluids I, H and L containing solely particles (I), (H) and (L), respectively. Parameters correspond to* $\mu = 1.34Pa \cdot s$, $\rho = 3.74\frac{g}{cm^3}$ *and* $\nu = 3.6 \cdot 10^{-4}\frac{m^2}{s}$.

Fluid	Viscosity	Density	Kin. Viscosity
I	μ	ρ	ν
H	1.54μ	ρ	1.54ν
L	0.55μ	ρ	0.55ν

5.2.2 Homogeneous fluid

The coarse grain model targets to reproduce a shear flow of a homogeneous fluid and consists of two particle types, (W) and (I), corresponding to the wall and fluid, respectively, as described in sect. 5.2.1. Particle interactions are governed by the LJ potential with parameters as in table 5.3.

Table 5.3: *List of LJ parameters for homogeneous fluid shear flow simulation. Parameters correspond to* $E = 0.250\ eV$, $\Sigma = 2.5\ \AA$.

Pair	ϵ	σ	R_c
(I)-(I)	E	Σ	4Σ
(W)-(W)	$3.6E$	Σ	4Σ
(I)-(W)	$2.8E$	Σ	4Σ

A sufficiently higher value -compared to that of the fluid particle interaction- of potential well depth is set to describe the interactions between the particles of the wall. The same parameter is also significantly higher for the interactions between the fluid particles and the wall particles compared to that of the fluid-fluid interaction in order to approximate the no-slip condition between the walls and the fluid. The wall particles are arranged according to a square unit cell lattice configuration. In specific, two basis particles are used, one at the corner and the other at the centre of the square.

The total simulation time is 50 ns with a time step of 1.0 fs. The fluid particles are implemented by a random placement in the domain between the walls. After their placement, a potential energy minimization of the system is performed, by iteratively adjusting particle coordinates. Once a local potential energy minimum is found, a constant velocity V_x is applied to the bottom wall.

5.2.3 Inhomogeneous fluid

The simulation model targets to reproduce the shear flow of an inhomogeneous fluid as in the continuum domain, fig. 3.9a. As shown in sect. 3.2, the relative friction reduction is independent of the plate distance, as long as the non-dimensional transversal viscosity distribution remains constant. Based on this, a three layer configuration is sought, in the nano-scale, with high viscosity layers near the two walls separated by a low viscosity one. Due to the fact that viscosity follows a continuous description in the continuum domain, a quantification of the layers' height needs to be made on a particle-based approach. It is assumed that, on a continuum basis, the high viscosity layer corresponds to the height of the slider on which the viscosity is at least 60% of its maximum value. Based on the optimized solution, this height is 20% of the distance between the plates. Therefore, in terms of particles, 20% of the total number of fluid particles, are used to reproduce each high viscosity layer and 60% the low viscosity one.

Based on the above, 700 particles of type (H) and 900 particles of type (L) are used to reproduce the fluid. The LJ parameters used to describe each pair of particles' interaction is shown in table 5.4.

Table 5.4: *List of LJ parameters for inhomogeneous fluid shearing flow simulation. Parameters correspond to* $E = 0.250\ eV$, $\Sigma = 2.5\ \mathring{A}$.

Pair	ϵ	σ	R_c
(H)-(H)	$1.2E$	Σ	4Σ
(L)-(L)	$0.8E$	Σ	4Σ
(H)-(L)	$0.6E$	Σ	1.12Σ
(W)-(W)	$3.6E$	Σ	4Σ
(H)-(W)	$2.8E$	Σ	4Σ
(L)-(W)	$0.2E$	Σ	1.12Σ

As seen from table 5.4, a small repulsive interaction ($R_c = 1.12\sigma$) is set for the pairs (H)-(L) and (L)-(W) in order to minimize mixing of the two fluids during the shearing process and, thus, maintain a non-homogeneous viscosity distribution spanwise.

The simulation is carried out similarly to the homogeneous fluid, as described in sect. 5.2.2. Fluid particles are implemented by a random placement in the domain between the walls with 50% of the (H) particles placed close to the bottom wall and 50% close to the top wall. As an extra measure against potential mixing of fluid particles (H) and (L), a small repulsive interaction is set among the (H) particles belonging to the different (top and bottom) layers. After their random placement, a potential energy minimization of the system is performed, after which a constant velocity V_x is applied to the bottom wall.

5.2.4 Results

Snapshots of the simulation box are shown in figs. 5.3 and 5.4 for two time instants, for the homogeneous and inhomogeneous fluid shear flow, respectively. As can be seen from the different colors of the same particles in fig. 5.3, a complete homogenization is achieved. On the other hand, as shown in fig. 5.4, a three-layer film is achieved with particles (H) sticking at the walls and particles (L) staying in the middle.

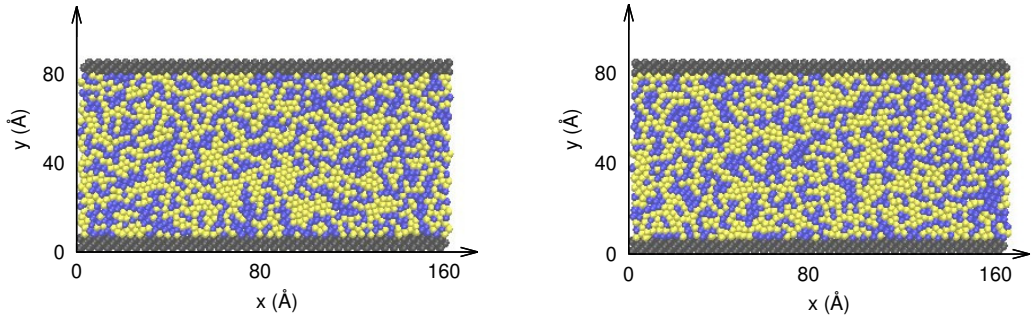

(a) *Time instant t.* **(b)** *Time instant $t + dt$.*

Figure 5.3: *Snapshots of the homogeneous fluid flow between parallel plates at two distinct time instants. Wall particles (W) are displayed in dark grey while fluid particles (I) in blue and yellow. Different colour is used for the fluid particles to emphasize the homogeneity of the fluid.*

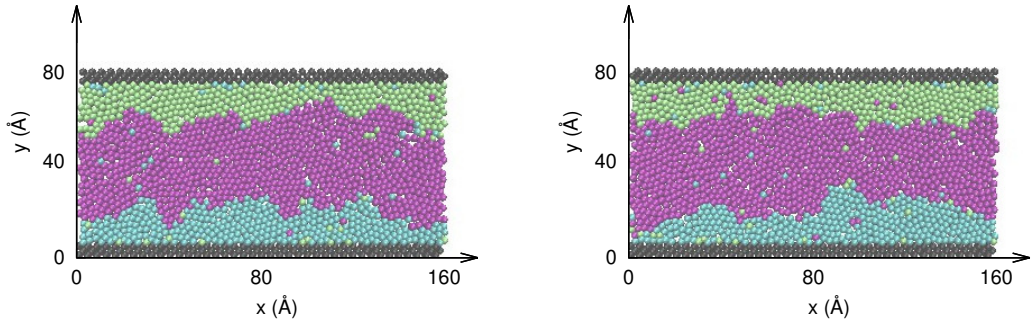

(a) *Time instant t.* **(b)** *Time instant $t + dt$.*

Figure 5.4: *Snapshots of the inhomogeneous fluid flow between parallel plates at two distinct time instants. Wall particles (W) are displayed in dark grey, fluid particles (H) in green and cyan and fluid particles (L) in purple.*

Throughout the simulation, tangential to the wall force data are stored. Since the simulations involve a random placement of particles, 5 independent trajectories are simulated for each case. Statistical analysis is carried out after the first 10 ns of the

simulation and for all trajectories, for tangential to the wall force and velocity results. A 45% decrease in the tangential force is found for the inhomogeneous fluid compared to the homogeneous one. It is shown that, even on the nano-scale, an inhomogeneity in the form of viscosity variations normal to the walls could potentially decrease the friction of the lubricated walls.

Even though the Green-Kubo computations showed that particles (H), (L) and (I) correspond to viscosities consistent with the continuum analysis, the interactions between different particle types in the shear flow simulations are bound to change the bulk liquid viscosities. Nevertheless, a fluid's effective viscosity is a quantification measure of its resistance to flow. Therefore, in order to further study the viscosity of the two films, velocity profile results are shown in fig. 5.5.

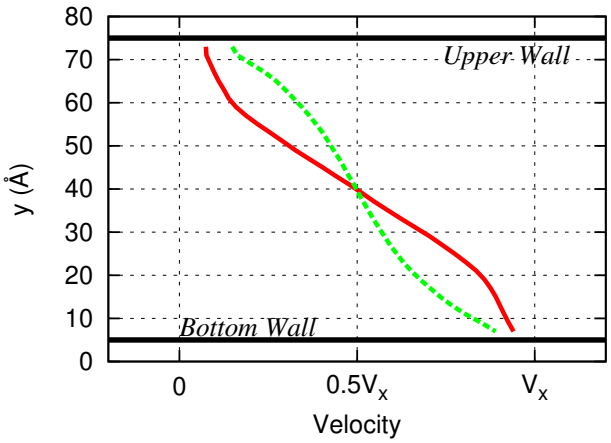

Figure 5.5: *Statistically time-averaged velocity profiles along the film thickness. Comparison between the homogeneous and inhomogeneous fluid. Continuous (red) line corresponds to the inhomogeneous fluid results, dashed (green) line to the homogeneous ones.*

The homogeneous fluid flow corresponds to a Couette-like flow and the velocity along the film thickness is approximated by a linear increase from the immobilized top wall to the moving bottom wall. On the other hand, the inhomogeneous fluid flow exhibits two zones of lower shear rate for heights equal to approximately 20% of the total height of the fluid domain. From results presented in table 5.2 and fig. 5.5, simulation described in sect. 5.2.3 is deemed to exhibit an inhomogeneous behaviour, in the form of significant viscosity variations normal to the walls.

Finally, comparing the velocity results of the particle-based description (fig. 5.5) with that of the continuum analysis (fig. 3.9b), a coherent velocity behaviour is observed through the scales for inhomogeneous-viscosity media. It is, thus, shown that nano-scale phenomena related to confined flows can be studied, to a certain extent, by continuum models as long as the implemented material's properties are consistent with the peculiarities and complexities of the nano-scale.

Chapter 6

Overview and Conclusions

6.1 Overview

In this diploma thesis, fluids with inhomogeneities and anisotropies are studied for potential implementation in lubricating engineering systems. The description of viscosity, in the classical N-S equations, is altered accordingly in order to emulate an inherently inhomogeneous or anisotropic media. For an inhomogeneous one (chapter 3), a spatial viscosity distribution is applied through proper parameterization schemes that are programmed and implemented in the OpenFOAM environment. On the other hand, a tensorial viscosity is used to describe an anisotropic media (chapter 4).

In specific, a Bézier curve (sect. 3.1.1) is used to parameterize viscosity along the longitudinal direction of a conventional hydrodynamic slider while a piecewise linear interpolation scheme (sect. 3.2.1) is used for the transversal direction. Through the use of an evolutionary algorithm, viscosity profiles are optimized, w.r.t. the control points of each scheme, leading to minimum specific friction. Parallelized or metamodel-assisted optimizations are used depending on the computational budget set for each case.

On the anisotropic approach, a proposed model is presented and implemented in OpenFOAM. A tensor is used to describe viscosity, the terms of which are studied for potential benefits on lubrication.

Finally, based on the results of the optimized transversal viscosity distribution, the study is extended on the nano-scale (chapter 5). Specific particle typologies featuring viscosity inhomogeneities normal to the walls, are selected using coarse grain MD simulations. Viscosity computations are carried out for customized particles in order

to identify consistent variations to those of the optimized case on the continuum domain. After that, shear flows are simulated to evaluate whether or not such viscosity variations are beneficial to lubrication even on the nano-scale.

6.2 Conclusions

Through this thesis, preliminary designs and models of new lubricants minimizing specific friction are presented. Novel lubricating ideas are necessary not only for the automotive industry but also for the majority of engineering systems, considering the performance and environmental impact of poorly lubricated configurations. Based on the studies presented on previous chapters, the following conclusions are drawn:

1. Through the longitudinal non-uniform viscosity distribution of a fluid in hydrodynamic lubrication applications, this work presents beneficial results compared to an homogeneous lubricant. In specific, while there is little variation to friction, a significantly increased load capacity is reported. It is, thus, shown that by managing to sustain a high viscosity in the inlet and outlet of the slider, the problem of squeeze film is diminished. Higher loads can be applied on the lubricated surfaces without the system moving out of the hydrodynamic lubrication regime and into the "painful" dry regime.

2. On the case of transversal viscosity variability, an optimal configuration, consisting of high viscosity layers near the walls separated by a low viscosity one, is identified. The key mechanism leading to the optimized lubrication results compared to a usual homogeneous lubricant is shown to be the change in the velocity profile along the film thickness. In the case of a converging hydrodynamic slider, the shear rate values along the moving wall change sign leading to the minimization of the friction force. This beneficial mechanism is shown to exist for different converging ratios. Additionally, in a parallel plates case, a drastically decreased absolute value of shear rate near the walls compared to a homogeneous fluid, leading to significantly less friction, is found.

3. It is also shown that viscosity inhomogeneity could be safely ignored when the height of the total film thickness is markedly larger than the thickness of the high viscosity zone. Furthermore, if the proportionality between the total film thickness and the high viscosity thickness remains constant then the relative result is unaffected. Based on this, particle based simulations are carried out, where the total film thickness is reduced to the scale of nanometers. It is shown that by applying consistent viscosity distributions, benefits to lubrication exist even on the nano-scale. Therefore, this thesis presents coherent results in different scale computational analysis, showing potential for a two-scale approach. While macro-scale models cannot accurately predict complex

nano-scale phenomena, they can provide valuable insight to a particle based approach.

4. It is found that anisotropy, as applied in chapter 4, does not effectively change the lubricant's specific friction. However, it is expected that a coupled anisotropic-inhomogeneous approach could potentially depict beneficial results.

Appendix A

Molecular Dynamics Computations

Temperature

For a system in equilibrium at a given temperature T, the theorem of equipartition states that the average kinetic energy per particle is related to T as

$$\frac{m}{2}\langle v^2 \rangle = \frac{3}{2} k_B T \tag{A.1}$$

where k_B is Boltzmann's constant. In a MD simulation, a computation of temperature can be made through the total kinetic energy of the system using

$$T_K = \frac{1}{3Nk_B} \sum_i m_i v_i^2 \tag{A.2}$$

As the kinetic energy fluctuates in time so does the computed temperature. Therefore, it is called "instantaneous temperature". Usually if one simulates a sufficiently large number of particles, T_K converges to roughly constant values.

Pressure

Usually pressure is computed from the virial theorem

$$PV = Nk_bT + \frac{1}{3}\sum_{i=1}^{N}\langle \vec{r_i} \cdot \vec{F_i} \rangle \tag{A.3}$$

where N is the number of particles in the system, k_b the Boltzmann constant, T the temperature, V the volume of the system and $\vec{F_i}$ is the force acting on the i-th particle due to the interaction with all other particles in the system. The second term of the right hand side of eq.A.3 is the virial if divided by V.

Diffusion Coefficient

The diffusion coefficient can be computed from the mean squared displacement of the particles as

$$D = \lim_{t\to\infty} \frac{\langle [\vec{r}(t) - \vec{r}(0)]^2 \rangle}{6t} \tag{A.4}$$

Alternatively -as used in this thesis- the Green-Kubo [36] relation can be used. The diffusion coefficient is related to the integral of the velocity auto-correlation function through equation

$$D = \frac{1}{3}\lim_{t\to\infty} \int_0^t \langle \vec{v}(\tau) \cdot \vec{v}(0) \rangle d\tau \tag{A.5}$$

Simulations at Constant Temperature

In experimental conditions the temperature is usually fixed. There are various methods of 'fixing' the temperature in a MD simulation and are called thermostats. The simplest thermostat consists in a rescaling of all the velocities after each integration step. It can be expressed as

$$\vec{v_i}'(t) = \lambda \vec{v_i}(t) \tag{A.6}$$

where the factor λ is obtained from

$$\lambda = \sqrt{\frac{T_0}{T_K(t)}} \tag{A.7}$$

where $T_K(t)$ is the instantaneous temperature defined by eq. A.1 and T_0 is the desired temperature.

Another thermostat is the Nosé-Hoover [37] one. In this scheme, the system is brought in contact with a "thermal bath". The system plus the bath form a closed system, so their total energy is conserved. The system however exchanges energy with the bath. This thermostat is deterministic and time evolution is described by the following equations of motion

$$\ddot{\vec{r}_i} = \frac{\vec{F}_i}{m_i} - \gamma \vec{r}_i \tag{A.8}$$

$$\dot{\gamma} = \frac{1}{Q}\Big(\sum_i \frac{p_i^2}{m_i} - 3Nk_BT_0\Big) \tag{A.9}$$

Equation A.8 is the Newton equation with an additional friction term with a time-dependent "friction" coefficient equal to γ, whose time evolution is described by eq. A.9. This quantity can be either positive or negative in the course of time. If γ is positive, energy is taken from the system whereas, if negative energy is given to the system. Eqs. A.8 and A.9 follow from an extended Hamiltonian in which system and bath degrees of freedom are coupled.

Appendix B

LAMMPS

LAMMPS [38] is a classical MD code that models ensembles of particles in a liquid, solid or gaseous state. It can model atomic, polymeric, biological, solid-state (metals, ceramics, oxides), granular, coarse-grained or macroscopic systems using a variety of interatomic potentials and boundary conditions. It can model 2D or 3D systems with only a few particles up to millions or billions.

LAMMPS is designed for parallel computers, however it can be run in personal ones. It will run on any parallel machine that supports the MPI message-passing library. LAMMPS is written in C++ and is designed in a way that makes it easy to modify or extend with new capabilities, such as new force fields, atom types, boundary conditions or diagnostics.

In the most general sense, LAMMPS integrates Newton's equations of motion for a collection of interacting particles. It uses neighbor lists to keep track of nearby particles. The lists are optimized for systems with particles that are repulsive at short distance, so that the local density of particles never becomes too large.

On parallel machines, LAMMPS uses spatial-decomposition techniques to partition the simulation domain into small sub-domains of equal computational cost, one of which is assigned to each processor.

Appendix C

Flowcharts

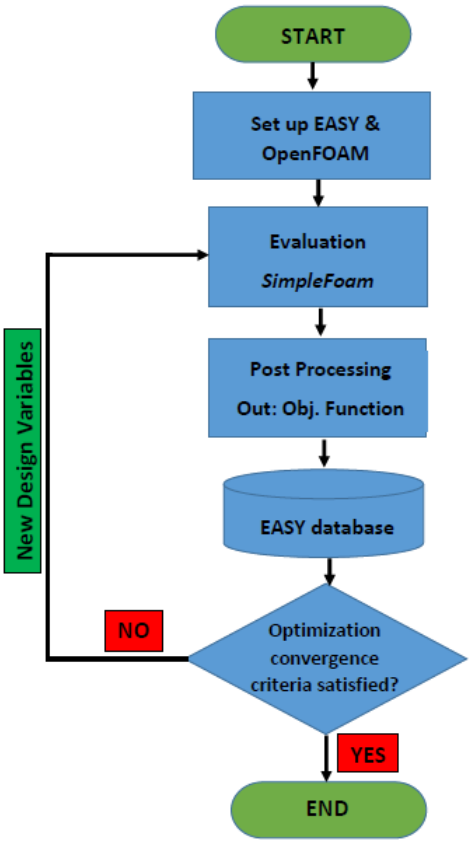

Figure C.1: *Optimization of inhomogeneous viscosity cases flowchart.*

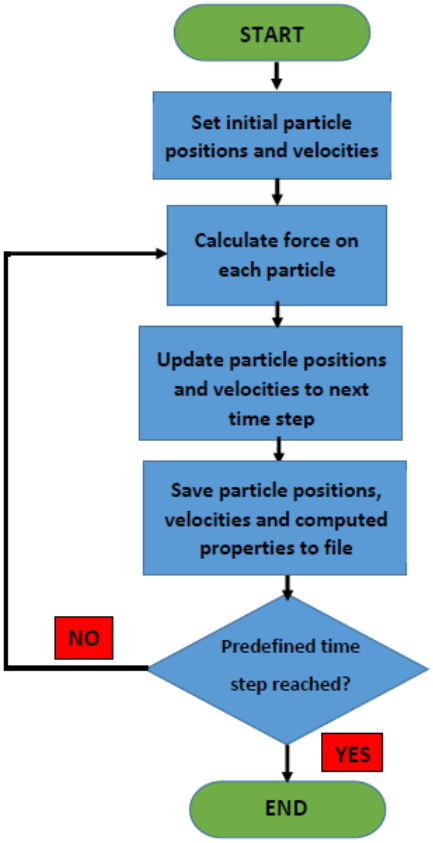

Figure C.2: *Molecular dynamics simulation flowchart.*

Bibliography

[1] W.Stachowiak, Gwidon and W.Batchelor, Andrew: *Engineering Tribology.* Butterworth-Heinemann, 2013.

[2] Holmeberg, K. and Erdemir, A.: *Influence of tribology on global energy consumption, costs and emissions.* Friction, 5(3):263–284, 2017.

[3] Robinson, J., Zhou, Y., Bhattacharya, P., and Erck, R.: *Probing the molecular design of hyper-branched aryl polyesters towards lubricant applications.* Scientific Reports, 6, 2016.

[4] Puccio, F. and Mattei, L.: *Biotribology of artificial hip joints.* World Journal of Orthopedics, 6(1):77–94, 2015.

[5] Reynolds, O.: *On the theory of lubrication and its application to mr. beauchamp tower's experiments, including an experimental determination of the viscosity of olive oil.* Philosophical Transactions of the Royal Society of London, 177:157–234, 1886.

[6] *Understanding how engines consume oil.* `http://www.machinerylubrication.com/Read/30384/engines-consume-oil`.

[7] Anderson, P., Tamminen, J., and Sandström, C.: *Piston ring tribology - a literature survey.* Espoo 2002. VTT Tiedotteita - Research Notes 2178. 105 p., December 3 2002.

[8] *Determining proper oil flow to journal bearings.* `http://www.machinerylubrication.com/Read/29654/journal-bearing-oil`.

[9] M.-D. Bermúdez, A.-E. Jiménez, J. Sanes and Carrión, F. J.: *Ionic liquids as advanced lubricant fluids.* Molecules, 14, 2009.

[10] B. Bhushan, J.N. Israelachvili and Landman, U.: *Nanotribology: friction, wear and lubrication at the atomic scale.* Nature, 374, 1995.

[11] S.J. Heo, S.B. Sinnott, D.W. Brenner and Harrison, J.A.: *Computational modeling of nanometer-scale tribology.* Springer Berlin Heidelberg, 2005.

[12] K. Gkagkas, V. Ponnuchamy et al.: *Molecular dynamics investigation of a model ionic liquid lubricant for automotive applications.* Tribol. Int., 113, 2017.

[13] A.C.F. Mendonça, A.A.H. Pádua and Malfreyt, P.: *Nonequilibrium molecular simulations of new ionic lubricants at metallic surfaces: Prediction of the friction.* J. Chem. Theory Comput., 9, 2013.

[14] C. Ye, W. Liu, Y. Chen and Yu, L.: *Room-temperature ionic liquids: a novel versatile lubricant.* Chem. Commun., 2001.

[15] C. Ye, W. Liu, Y. Chen and Ou, Z.: *Tribological behaviour of dy-sialon ceramics sliding against si_3n_4 under lubrication of fluorine-containing oils.* Wear, 253, 2002.

[16] Jiménez, A. E. and Bermúdez, M. D.: *Imidazolium ionic liquids as additives of the synthetic ester propylene glycole dioleate in aluminium-steel lubrication.* Wear, 265, 2008.

[17] Phillips, B.S. and Zabinski, J.S.: *Ionic liquid lubrication effects on ceramics in a water environment.* Tribol. Lett., 17, 2004.

[18] J. Qu, P.J. Blau, S. Dai et al.: *Ionic liquids as novel lubricants and additives for diesel engine applications.* Tribol. Lett., 35, 2009.

[19] E. Manias, G. Hadziioannou and Brinke, G.ten: *Inhomogeneities in sheared ultrathin lubricating films.* Langmuir, 12, 1996.

[20] Montfort, J.P. and Hadziioannou, G.

[21] Granick, S.: *Motions and relaxations of confined liquids.* Science, 253, 1991.

[22] A.I. Vakis, V.A. Yastrebov, J. Scheibert et al.: *Modeling and simulation in tribology across scales: An overview.* Tribol. Int., 125, 2018.

[23] D. Savio, K. Falk and Moseler, M.: *Slipping domains in water-lubricated microsystems for improved load support.* Tribol. Int., 120, 2018.

[24] Cosden, I.A. and Lukes, J.R.: *A hybrid atomistic-continuum model for fluid flow using lammps and openfoam.* Comput. Phys. Commun., 184, 2013.

[25] Kyle, J.P. and Terrell, E.J.: *Application of smoothed particle hydrodynamics to full-film lubrication.* J. Tribol., 135, 2013.

[26] Versteeg, H. K. and Malalasekera, W.: *An introduction to computational fluid dynamics. The finite volume method.* Addison–Wesley, 1996.

[27] Weller, H.G. and Tabor, G.: *A tensorial approach to computational continuum mechanics using object-oriented techniques.* Computers in Physics, 12, 1998.

[28] Papoutsis-Kiachagias, E.: *Adjoint Methods for Turbulent Flows, Applied to Shape or Topology Optimization and Robust Design.* PhD thesis, Laboratory of Thermal Turbomachines, NTUA, Athens, 2013.

[29] Giannakoglou, K.C: *Optimization Methods in Aerodynamics.* Notes. Laboratory of Thermal Turbomachines, NTUA, Athens, 2005.

[30] *Easy webpage*. http://velos0.ltt.mech.ntua.gr/EASY.

[31] Oldroyd, J.G.: *On the formulation of rheological equations of state*. Proceedings of the royal society A, 1950.

[32] Tobias Amann, Christian Dold and Kailer, Andreas: *Complex fluids in tribology to reduce friction: Mesogenic fluids, ionic liquids and ionic liquid crystals*. Tribol. Int., 65, 2013.

[33] *Icams webpage*. http://www.icams.de/content/research.

[34] Carlon, E.: *Computational Physics B*. Notes. Katholieke Universiteit, Leuven, 2010.

[35] S. Kmiecik, D. Gront et al: *Coarse-grained protein models and their applications*. Chemical Reviews, 116, 2016.

[36] Green, Melville S.: *Brownian motion in a gas of noninteracting molecules*. J. Chem. Phys., 19, 1951.

[37] Evans, D.J. and Holian, B.L.: *The nose-hoover thermostat*. J. Chem. Phys., 83, 1985.

[38] *Lammps manual*. http://lammps.sadvia.gov/doc/Manual.html.

Εθνικό Μετσόβιο Πολυτεχνείο
Σχολή Μηχανολόγων Μηχανικών
Τομέας Ρευστών
Μονάδα Παράλληλης Υπολογιστικής Ρευστοδυναμικής & Βελτιστοποίησης

Προκαταρτικός Σχεδιασμός Νέων Λιπαντικών με Ανομοιογενή ή Ανισότροπη Συνεκτικότητα

Διπλωματική Εργασία

Γεώργιος Μπλέτσος

Ακαδημαϊκός Επιβλέπων:
Κυριάκος Χ. Γιαννάκογλου, Καθηγητής ΕΜΠ

Βιομηχανικός Επιβλέπων:
Δρ. Κωνσταντίνος Γκαγκάς, Ειδικός Toyota Motor Europe

Αθήνα, Ιούνιος 2019

ΕΚΤΕΝΗΣ ΠΕΡΙΛΗΨΗ ΣΤΑ ΕΛΛΗΝΙΚΑ

Εισαγωγή

Οι δυνάμεις τριβής αντιστοιχούν σε περίπου 15% της ενέργειας του καυσίμου που χάνεται στα οχήματα με μηχανές εσωτερικής καύσης. Η περιβαλλοντική αλλά και οικονομική ανάγκη για μείωση αυτού του ποσοστού καθιστά τον σχεδιασμό νέων λιπαντικών αναγκαίο. Στην διπλωματική αυτή εργασία μελετούνται εφαρμογές υδροδυναμικής λίπανσης, κατά τις οποίες υδροδυναμικό φιλμ λιπαντικού παρεμβάλλεται μεταξύ δύο επιφανειών σε σχετική κίνηση.

Με βάση μοριακές μελέτες στα ιονικά υγρά ως λιπαντικά [1,2], τα οποία παρουσιάζουν εγγενείς ανομοιογένειες, και στους υγρούς κρυστάλλους [3], που παρουσιάζουν ανισότροπα χαρακτηριστικά, η διπλωματική εργασία στοχεύει στη μελέτη και βελτιστοποίηση ιδεατών λιπαντικών με ανομοιογενή ή ανισότροπη συνεκτικότητα. Για την ανάλυση ρευστών με ανομοιογενή συνεκτικότητα προγραμματίζονται και εισάγονται στο περιβάλλον OpenFOAM σχήματα παραμετροποίησης της συνεκτικότητας. Οι εξισώσεις προς επίλυση είναι οι Navier-Stokes. Με τη χρήση εξελικτικών αλγορίθμων,

μέσω του λογισμικού EASY, βελτιστοποιούνται τα πεδία συνεκτικότητας, με στόχο τη μείωση των χαρακτηριστικών τριβής του λιπαντικού.

Η ανισότροπη συμπεριφορά προσεγγίζεται με τη χρήση τανυστικής συνεκτικότητας. Στην κατεύθυνση αυτή, προγραμματίζεται επιλύτης της ροής που εισάγει την τανυστική περιγραφή της συνεκτικότητας. Η μελέτη επεκτείνεται στην κλίμακα των νανομέτρων. Με έναυσμα τη μελέτη στον συνεχή χώρο και τη χρήση προσομοιώσεων μοριακής δυναμικής, διερευνάται η δυνητική βελτίωση των χαρακτηριστικών τριβής σε ακραίες καταστάσεις λίπανσης.

Η γεωμετρία στην οποία αναλύεται η στρωτή, ισοθερμοκρασιακή ροή, ασυμπίεστου ρευστού είναι αυτή του σχ. 1.

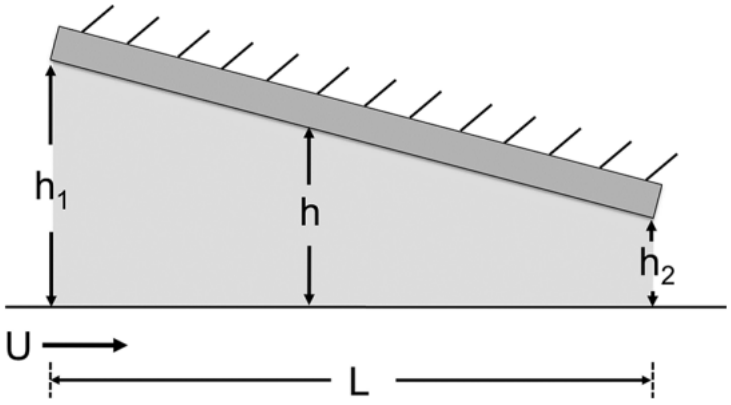

Σχήμα 1: *Σχηματικό τυπικού συγκλίνοντος υδροδυναμικού ολισθητή [4].*

Κατανομή Συνεκτικότητας στη Διαμήκη Διεύθυνση

Η συνεκτικότητα παραμετροποιείται στη διαμήκη διεύθυνση του υδροδυναμικού ολισθητή με χρήση καμπύλης Bézier τριών σημείων ελέγχου. Συγκεκριμένα, το σχήμα παραμετροποίησης προγραμματίζεται έτσι ώστε να υπάρχει έλεγχος της κατώτατης δυνατής τιμής ($3 \cdot 10^{-7}$ $\frac{m^2}{s}$) και της μέση τιμής ($3 \cdot 10^{-6}$ $\frac{m^2}{s}$), από τον χρήστη. Με τον τρόπο αυτό αποφεύγονται αφύσικες τιμές της συνεκτικότητας (μηδενικές ή αρνητικές) και δημιουργείται η δυνατότητα για σύγκριση με αντίστοιχο ομογενές ρευστό. Στην συνέχεια με χρήση εξελικτικών αλγορίθμων εντοπίζονται κατανομές συνεκτικότητας οι οποίες μειώνουν τον λόγο της εφαπτομενικής δύναμης προς την κάθετη δύναμη στον κινούμενο τοίχο. Η βελτιστοποιημένη κατανομή, όπως φαίνεται στο σχ. 2, οδήγησε σε 27% μείωση του $SF = \frac{F_x}{F_y}$, σε σχέση με αντίστοιχο ομογενές ρευστό.

Κατανομή Συνεκτικότητας στην Εγκάρσια Διεύθυνση

Το σχήμα παραμετροποίησης που προγραμματίζεται, αποτελείται απο 11 σημεία ελέγχου γραμμικώς συνδεόμενα μεταξύ τους. Ομοίως με προηγουμένως, υπάρχει έλεγχος της

κατώτατης και μέσης τιμής, από τον χρήστη, όπου για τη διαδικασία βελτιστοποίησης επιλέγονται ίδιες τιμές με την περίπτωση της κατανομής στη διαμήκη κατεύθυνση. Η διαδικασία βελτιστοποίησης υποβοηθείται από χαμηλού κόστους προσεγγιστικά πρότυπα αξιολόγησης. Η βελτιστοποιημένη κατανομή, όπως φαίνεται στο σχ. 3, οδήγησε σε 65% μείωση του SF, σε σχέση με αντίστοιχο ομογενές ρευστό.

Αποτελέσματα Βελτιστοποίησης Ανομοιογενούς Συνεκτικότητας

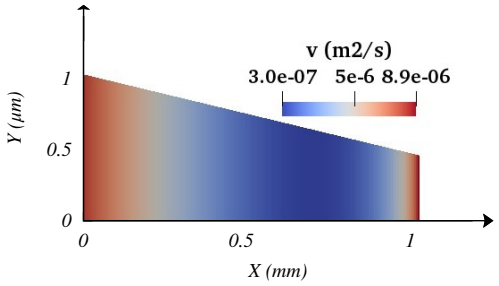

(α′) *Βελτιστοποιημένες περιοχές ισο-ν, με υψηλή συνεκτικότητα στην είσοδο και έξοδο του ολισθητή και χαμηλή στο ενδιάμεσο.*

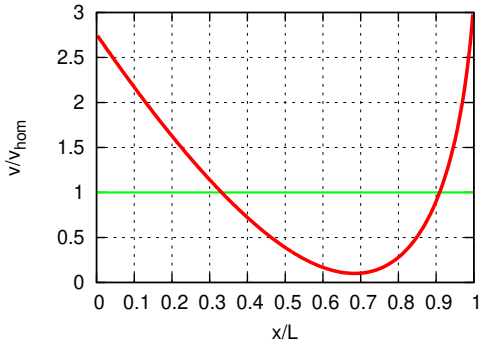

(β′) *Βελτιστοποιημένη καμπύλη Bézier. Η τιμή $\nu_{hom} = \nu_{ave}$ αντιστοιχεί στην τιμή συνεκτικότητας του ομογενούς ρευστού.*

Σχήμα 2: *Αποτελέσματα βελτιστοποίησης για κατανομή της συνεκτικότητας στη διαμήκη διεύθυνση του ολισθητή.*

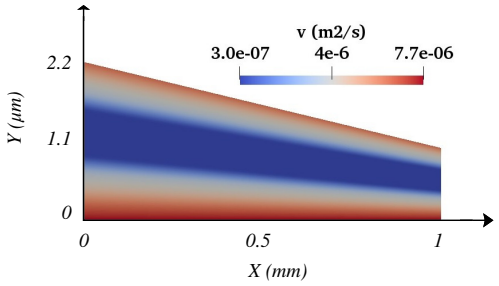

(α′) *Βελτιστοποιημένες περιοχές ισο-ν, με υψηλή συνεκτικότητα κοντά στα στερεά τοιχώματα του ολισθητή και χαμηλή στο ενδιάμεσο.*

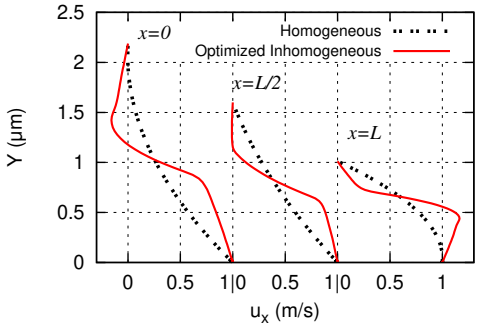

(β′) *Κατανομή ταχυτήτων κατά μήκος του ολισθητή. Σύγκριση μεταξύ του ομογενούς και ανομοιογενούς ρευστού.*

Σχήμα 3: *Αποτελέσματα βελτιστοποίησης για κατανομή της συνεκτικότητας στην εγκάρσια διεύθυνση του ολισθητή.*

Ανισότροπο Μοντέλο

Για τη δημιουργία του μοντέλου, γίνεται η υπόθεση ότι η σχέση μεταξύ του τανυστή συνεκτικών τάσεων (τ_{ij}) και των παραγώγων της ταχύτητας ($\frac{\partial v_i}{\partial x_j}$) είναι γραμμική. Συγκεκριμένα,

$$\begin{aligned}\tau_{ij} =& C_{ijlm}\frac{\partial v_l}{\partial x_m} \\ \tau_{ij} =& (c_{ijlm} + \nu_{ijlm})\frac{\partial v_l}{\partial x_m}\end{aligned}$$

όπου,

$$c_{ijlm} = \nu_c(\delta_{il}\delta_{jm} + \delta_{im}\delta_{jl})$$

Εισάγοντας την παραπάνω διατύπωση στις εξισώσεις Navier-Stokes προκύπτει η ακόλουθη τανυστική έκφραση των εξισώσεων ορμής:

$$v_j\frac{\partial v_i}{\partial x_j} - \frac{\partial}{\partial x_j}\Big[\nu_c\Big(\frac{\partial v_i}{\partial x_j} + \frac{\partial v_j}{\partial x_i}\Big)\Big] + \frac{\partial p}{\partial x_i} - \frac{\partial}{\partial x_j}\Big(A_{ij}\Big) = 0, \quad i,j = 1,2 \tag{1}$$

όπου $A_{ij} = \nu_{ijlm}\frac{\partial v_l}{\partial x_m}$.

Έτσι, με την παραπάνω μεθοδολογία, δίνεται η δυνατότητα ελέγχου των ΄κυρίαρχων΄ χαρακτηριστικών του ρευστού, μέσω του όρου c_{ijlm} και των αποκλίσεων από αυτά λόγω της δυνητικής ανισότροπης συμπεριφοράς, μέσω του όρου ν_{ijlm}.

Ανάπτυξη Επιλύτη SimpleAnisoFoam

Όπως φαίνεται από την εξίσωση 1, η διατύπωση των εξισώσεων της ορμής αποτελείται από την κλασική διατύπωση των Navier-Stokes και ενός ανισότροπου όρου A_{ij}. Για την υλοποίηση του επιλύτη της ροής, λοιπόν, μεταβάλλεται ο ήδη υπάρχων αλγόριθμος simpleFoam, επίλυσης της ροής ασυμπίεστων ρευστών, με την εισαγωγή του ανισότροπου όρου.

Συγκεκριμένα, απαιτούνται από τον χρήστη τα ίδια αρχεία εισόδου με αυτά του simpleFoam. Επιπλέον απαιτούνται τα (αδιάστατα) στοιχεία τεσσάρων, δεύτερης τάξης τανυστών (C^{ij}_{lm}), όπου κατασκευάζονται από προ-επεξεργαστή. Οι τανυστές αυτοί πολλαπλασιάζονται με την τιμή ν_c, της εξίσωσης 1 και, στη συνέχεια, χρησιμοποιούν-

ται για την κατασκευή του όρου A_{ij}. Αναλυτικά, ο όρος προκύπτει ως εξής:

$$A_{ij} = C_{lm}^{ij} : \frac{\partial v_l}{\partial x_m}$$

Προσομοιώσεις Μοριακής Δυναμικής

Η έρευνα επεκτείνεται στην κλίμακα των νανομέτρων με χρήση προσομοιώσεων μοριακής δυναμικής. Στόχος είναι η μελέτη πιθανής μείωσης των δυνάμεων τριβής σε ακραίες καταστάσεις λίπανσης, στις οποίες η παραδοχή συνεχούς χώρου καταρρέει. Μέσω αυτής της διαδικασίας δίνονται, επίσης, ιδέες για πιο εκτενή σχεδιασμό του βελτιστοποιημένου λιπαντικού. Συγκεκριμένα, οι προσομοιώσεις μοριακής δυναμικής στοχεύουν να επεκτείνουν τη μελέτη που πραγματοποιήθηκε για ανομοιογενή ρευστά, με κατανομή συνεκτικότητας στην εγκάρσια διεύθυνση του ολισθητή.

Η βασική ιδέα της μοριακής δυναμικής είναι η αριθμητική ολοκλήρωση στον χρόνο των κλασικών εξισώσεων κίνησης, με σκοπό να παράγουν την τροχιά ενός συστήματος αποτελούμενου από N σωματίδια. Η αλληλεπίδραση των σωματιδίων προσομοιώνεται μέσω του δυναμικού Lennard-Jones, σύμφωνα με το οποίο

$$V_{LJ}(r) = 4\epsilon\Big[(\frac{\sigma}{r})^{12} - (\frac{\sigma}{r})^{6}\Big] \tag{2}$$

Χαρακτηριστικά μεγέθη της εξίσωσης 2 είναι η απόσταση μηδενικού δυναμικού σ και το βάθος του ενεργειακού πηγαδιού ϵ.

Η δύναμη μεταξύ των σωματιδίων περιγράφεται από την εξίσωση:

$$F = -\nabla V_{LJ} \tag{3}$$

Με βάση την μελέτη στον συνεχή χώρο, δημιουργούνται 2 είδη εικονικών σωματιδίων, ένα υψηλής συνεκτικότητας και ένα χαμηλής. Δημιουργείται επίσης εικονικό σωματίδιο για την περιγραφή ομογενούς ρευστού, με τιμή συνεκτικότητας ενδιάμεση των προηγούμενων δύο. Έπειτα, κατασκευάζονται δύο μοντέλα ροής, ένα για το ανομοιογενές ρευστό και ένα για το ομοιογενές. Πραγματοποιούνται προσομοιώσεις για 50ns, κατά τη διάρκεια των οποίων αποθηκεύονται οι εφαπτομενικές δυνάμεις στο στερεό τοίχωμα.

Παρατηρείται ότι το μοντέλο ανομοιογενούς ρευστού παρουσίασε 45% μείωση της δύναμης τριβής στα στερεά τοιχώματα σε σχέση με το μοντέλο ομοιογενούς ρευστού. Στιγμιότυπα των δύο υπολογιστικών μοντέλων παρουσιάζονται στα σχ. 4 & 5. Συγκρίνονται επίσης οι κατανομές ταχυτήτων των δύο ροών στο σχ. 6.

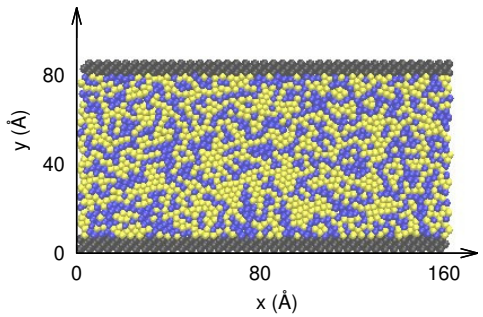

(α′) *Χρονική στιγμή* t.

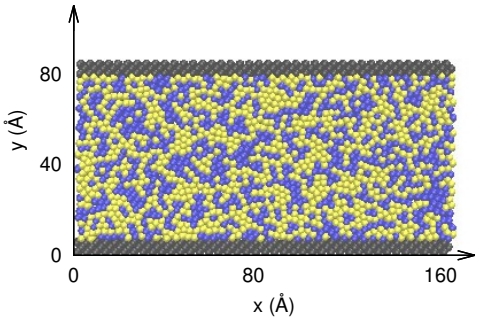

(β′) *Χρονική στιγμή* $t + dt$.

Σχήμα 4: *Χρονικά στιγμιότυπα ροής ομογενούς ρευστού ανάμεσα σε παράλληλες πλάκες. Τα σωματίδια του τοίχου παρουσιάζονται με σκούρο γκρι χρώμα ενω τα σωματίδια του ρευστού με μπλε και κίτρινο. Ο διαφορετικός χρωματισμός των ίδιων σωματιδίων του ρευστού γίνεται με στόχο να φανεί η ομοιογένεια.*

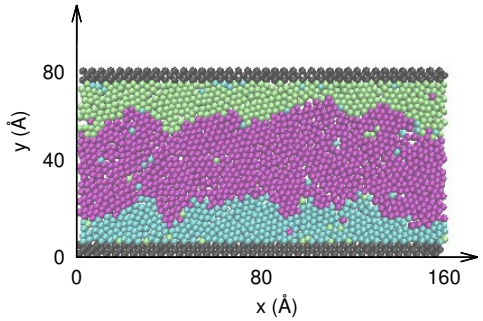

(α′) *Χρονική στιγμή* t.

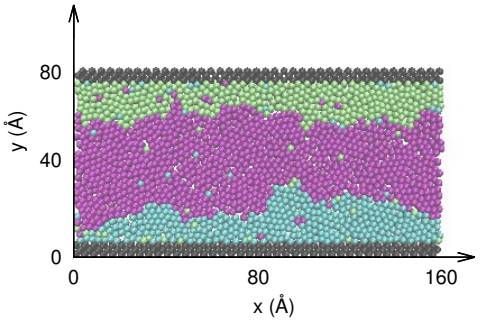

(β′) *Χρονική στιγμή* $t + dt$.

Σχήμα 5: *Χρονικά στιγμιότυπα ροής ανομοιογενούς ρευστού ανάμεσα σε παράλληλες πλάκες. Τα σωματίδια υψηλής συνεκτικότητας χρωματίζονται με πράσινο και κυανό ενώ αυτά με χαμηλή συνεκτικότητα με μωβ.*

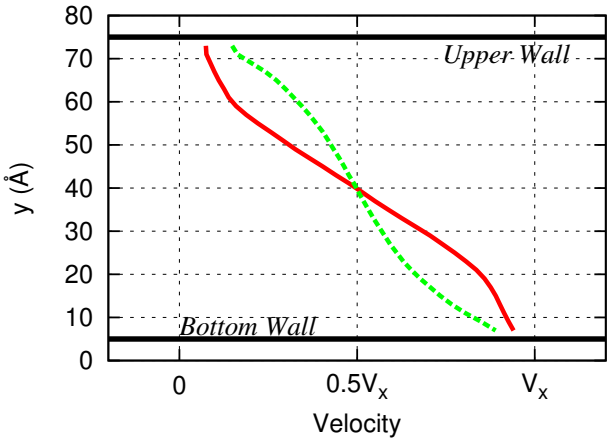

Σχήμα 6: *Κατανομές ταχύτητας καθ'ύψος του υδροδυναμικού φιλμ. Σύγκριση μεταξύ του ομογενούς και ανομοιογενούς ρευστού. Η συνεχής (κόκκινη) γραμμή αντιστοιχεί στο ανομοιογενές ρευστό, η ασυνεχής (πράσινη) γραμμή στο ομοιογενές.*

Επιπλέον Αποτελέσματα στον Συνεχή Χώρο

Πραγματοποιούνται, επίσης, παραμετρικές μελέτες στον συνεχή χώρο για την περίπτωση των παράλληλων πλακών. Συγκεκριμένα, χρησιμοποιώντας την κατανομή στην εγκάρσια διεύθυνση που βρέθηκε μέσω της διαδικασίας βελτιστοποίησης, προσομοιώνονται και συγκρίνονται ροές ομογενούς και ανομοιογενούς ρευστού. Παρατηρείται πως, στην περίπτωση των παράλληλων πλακών, η τριβή στις πλάκες μειώνεται κατά 73% με χρήση του βελτιστοποιημένου ανομοιογενούς ρευστού.

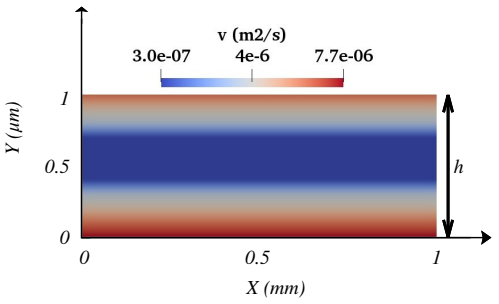

(α′) *Βελτιστοποιημένες περιοχές ισο-ν για την περίπτωση παράλληλων πλακών.*

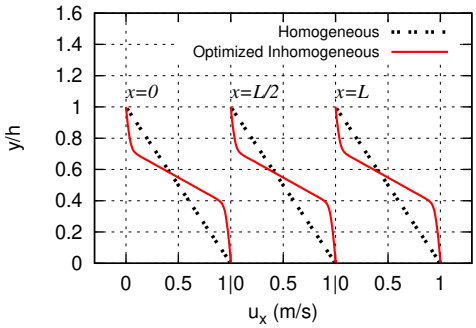

(β′) *Κατανομές ταχυτήτων.*

Σχήμα 7: *Αποτελέσματα προσομοιώσεων παράλληλων πλακών.*

Τέλος, παρουσιάζονται αποτελέσματα μελέτης της επίδρασης του συνολικού ύψους του ολισθητή, για την περίπτωση παράλληλων πλακών, καθώς και του λόγου σύγκλισης, για την περίπτωση συγκλίνοντος ολισθητή.

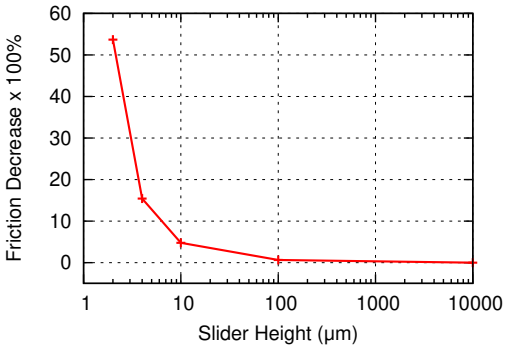

(α′) *Αποτελέσματα τριβής για διαφορετικά ύψη h.*

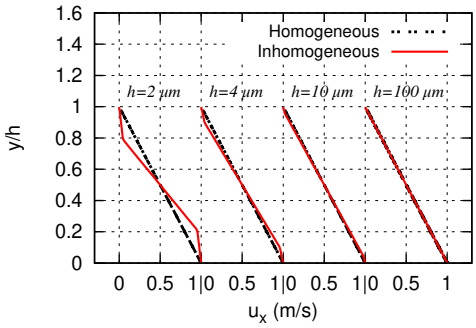

(β′) *Κατανομές ταχυτήτων για διαφορετικά ύψη h. Καθώς αυξάνει το συνολικό ύψος της γεωμετρίας, δεν παρατηρούνται σημαντικές διαφορές ανάμεσα στο ομοιογενές και ανομοιογενές ρευστό.*

Σχήμα 8: *Αποτελέσματα παραμετρικής μελέτης για διαφορετικά ύψη h.*

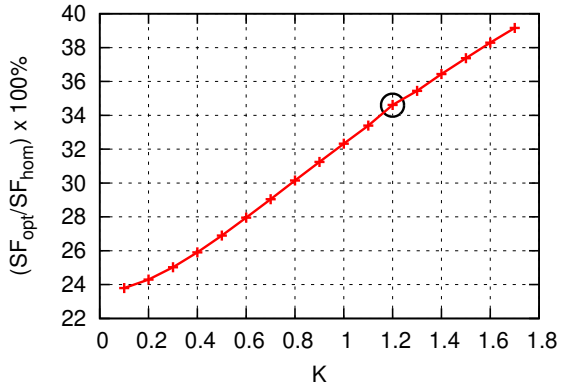

Σχήμα 9: *Μείωση του SF ως προς το ομοιογενές ρευστό για διαφορετικούς λόγους σύγκλισης K. Ο κύκλος αντιστοιχεί στον λόγο σύγκλισης που πραγματοποιήθηκε η βελτιστοποίηση.*

Σύνοψη-Συμπεράσματα

Στην διπλωματική αυτή εργασία μελετούνται ρευστά με ανομοιογενή ή ανισότροπη συνεκτικότητα με στόχο τον δυνητικό σχεδιασμό τους για χρήση σε μηχανολογικά συστήματα λίπανσης. Στην περίπτωση των ανομοιογενών ρευστών, η συνεκτικότητα κατανέμεται στον χώρο μέσω σχημάτων παραμετροποίησης τα οποία προγραμματίζονται και εισάγονται στο περιβάλλον OpenFOAM. Για τα ανισότροπα ρευστά, προγραμματίζεται επιλύτης της ροής ο οποίος δίνει την δυνατότητα στον χρήστη να περιγράψει με τανυστική μορφή την συνεκτικότητα. Τέλος, με βάση τα αποτελέσματα απο τη μελέτη στον συνεχή χώρο, η έρευνα επεκτείνεται στην κλίμακα των νανομέτρων με τη χρήση προσομοιώσεων μοριακής δυναμικής.

Με βάση τα αποτελέσματα που παρουσιάζονται στην εργασία, καταλήγουμε στα εξής συμπεράσματα:

1. Στην περίπτωση της βελτιστοποιημένης κατανομής της συνεκτικότητας στην εγκάρσια διεύθυνση, παρατηρείται υψηλή συνεκτικότητα κοντά στα στερεά τοιχώματα με ένα στρώμα χαμηλής συνεκτικότητας να παρεμβάλλεται. Η βελτιστοποιημένη κατανομή δοκιμάζεται και σε διαφορετικές γεωμετρίες, όπου διατηρεί τα θετικά αποτελέσματα σε σχέση με αντίστοιχο ομογενές ρευστό.
2. Συμπεραίνουμε πως η ανομοιογένεια της συνεκτικότητας μπορεί να αμεληθεί όταν το ύψος του υδροδυναμικού ολισθητή είναι σημαντικά μεγαλύτερο από τη ζώνη υψηλής συνεκτικότητας.
3. Παρουσιάζονται συναφή αποτελέσματα σε μελέτες διαφορετικής κλίμακας. Φαίνεται, λοιπόν, πως, παρόλο που τα μοντέλα του συνεχούς χώρου δεν μπορούν να περιγράψουν επακριβώς τις ιδιαιτερότητες του μικρόκοσμου, μπορούν να προσφέρουν σημαντική πληροφορία σε μία ανάλυση σωματιδίων.

Επιλεγμένη Βιβλιογραφία

[1] K. Gkagkas, V. Ponnuchamy et al.:*Molecular dynamics investigation of a model ionic liquid lubricant for automotive applications.* Tribol. Int., 113, 2017.

[2] C. Ye, W. Liu, Y. Chen and Yu, L.:*Room-temperature ionic liquids: a novel versatile lubricant.* Chem. Commun., 2001.

[3] T. Amann, C. Dold and Kailer, A.:*Complex fluids in tribology to reduce friction: Mesogenic fluids, ionic liquids and ionic liquid crystals.* Tribol. Int., 65, 2013.

[4] Kyle, J.P. and Terrell, E.J.:*Application of smoothed particle hydrodynamics to full-film lubrication.* J. Tribol., 135, 2013.

[5] Carlon, E.:*Computational Physics B.* Notes. Katholieke Universiteit, Leuven, 2010.